NAVAL POSTGRADUATE SCHOOL
MONTEREY, CALIFORNIA

THESIS

OPTIMAL LINEAR QUADRATIC GAUSSIAN CONTROLLER DESIGN FOR A FLEXIBLE-SPACECRAFT SIMULATOR

by

William Burke Harrington, Jr.

December 1995

Thesis Advisor: **Roberto Cristi**

Approved for public release; distribution is unlimited.

REPORT DOCUMENTATION PAGE

Form Approved OMB No. 0704-0188

1. AGENCY USE ONLY *(Leave blank)*	2. REPORT DATE December 1995	3. REPORT TYPE AND DATES COVERED Master's Thesis

4. TITLE AND SUBTITLE
OPTIMAL LINEAR QUADRATIC GAUSSIAN CONTROLLER DESIGN FOR A FLEXIBLE-SPACECRAFT SIMULATOR

5. FUNDING NUMBERS

6. AUTHOR(S)
Harrington, William Burke Jr.

7. PERFORMING ORGANIZATION NAME(S) AND ADDRESS(ES)
Naval Postgraduate School
Monterey CA 93943-5000

8. PERFORMING ORGANIZATION REPORT NUMBER

9. SPONSORING/MONITORING AGENCY NAME(S) AND ADDRESS(ES)

10. SPONSORING/MONITORING AGENCY REPORT NUMBER

11. SUPPLEMENTARY NOTES The views expressed in this thesis are those of the author and do not reflect the official policy or position of the Department of Defense or the U.S. Government.

12a. DISTRIBUTION/AVAILABILITY STATEMENT
Approved for public release; distribution is unlimited.

12b. DISTRIBUTION CODE

13. ABSTRACT *(maximum 200 words)*

The experimental verification of active control methods for vibration suppression of large flexible structures in space is essential for precision optical and military payload operations. The Flexible-Spacecraft Simulator (FSS) at the Naval Postgraduate School is designed for testing such control designs. The experimental setup simulates the pitch axis motion of a rigid body spacecraft with a flexible antenna support structure connected to a rigid reflector. A twenty-four state finite element analytical model is used to characterize the flexible appendage. Piezoelectric sensors and actuators are used for feedback control for vibration suppression. In addition, an external infrared camera provides direct feedback of the flexible structure's elbow and tip displacements and rotations. A Multiple-Input-Multiple-Output (MIMO) linear quadratic gaussian (LQG) controller is designed using linear quadratic regulator (LQR) optimal control theory and an optimal Kalman estimator as the state observer to meet desired performance specifications. The objective is to minimize the motion of the reflector.

14. SUBJECT TERMS Optimal control, Linear Quadratic Regulator, LQR, Linear Quadratic Gaussian, LQG, Smart Structures, Simulation	15. NUMBER OF PAGES 89
	16. PRICE CODE

17. SECURITY CLASSIFICATION OF REPORT	18. SECURITY CLASSIFICATION OF THIS PAGE	19. SECURITY CLASSIFICATION OF ABSTRACT	20. LIMITATION OF ABSTRACT
Unclassified	Unclassified	Unclassified	UL

NSN 7540-01-280-5500 Standard Form 298 (Rev. 2-89)

Prescribed by ANSI Std. 239-18 298-102

Approved for public release; distribution is unlimited.

OPTIMAL LINEAR QUADRATIC GAUSSIAN CONTROLLER DESIGN FOR A FLEXIBLE SPACECRAFT SIMULATOR

William Burke Harrington, Jr.
Lieutenant Commander, United States Navy
B. S. Marine Engineering, U. S. Naval Academy, 1985

Submitted in partial fulfillment
of the requirements for the degree of

MASTER OF SCIENCE IN ELECTRICAL ENGINEERING

from the

NAVAL POSTGRADUATE SCHOOL
December 1995

Author: _____
William Burke Harrington, Jr.

Approved by: _____
Roberto Cristi, Thesis Advisor

_____
Brij N. Agrawal, Second Reader

_____
Herschel H. Loomis, Jr., Chairman
Department of Electrical and Computer Engineering

ABSTRACT

The experimental verification of active control methods for vibration suppression of large flexible structures in space is essential for precision optical and military payload operations. The Flexible-Spacecraft Simulator (FSS) at the Naval Postgraduate School is designed for testing such control designs. The experimental setup simulates the pitch axis motion of a rigid body spacecraft with a flexible antenna support structure connected to a rigid reflector. A twenty-four state finite element analytical model is used to characterize the flexible appendage. Piezoelectric sensors and actuators are used for feedback control for vibration suppression. In addition, an external infrared camera provides direct feedback of the flexible structure's elbow and tip displacements and rotations. A Multiple-Input-Multiple-Output (MIMO) linear quadratic gaussian (LQG) controller is designed using linear quadratic regulator (LQR) optimal control theory and an optimal Kalman estimator as the state observer to meet desired performance specifications. The objective is to minimize the motion of the reflector.

TABLE OF CONTENTS

AKNOWLEDGEMENTS

I would like to acknowledge those people that made this endeavor possible. First of all, my wife, Angela deserves the majority of the credit for this work. She is the one who stayed up nights with our two young children, she is the one that sacrificed her free time for me to come in and put in the extra hours required to complete these degrees and, she is the one who had unwavering faith in my abilities here at NPS. This thesis would not have been possible without her full and loving support. Next, my thesis advisors, Professor Cristi and Professor Agrawal; they backed me up when the time came to present my work and they encouraged me when times got tough. I learned a great deal from them not only academically but on how to be optimistic when the pressure is on. I will always be grateful for their support and encouragement. Last, but not least, is Doctor John Meyer. John came in on weekends to help me past the trouble spots in my work and sacrificed a good portion of his workday to help me get my thesis in on time.

I. INTRODUCTION

The rapid advancement of space sensor technology and the requirement for nanometer accuracy has created a need for minimum vibration noise, high precision mounting platforms from space. The consumer's demand for high resolution imagery, large space structures, and precise position and attitude determination has produced a large amount of advanced research in the field of structural control. Concurrent to the rapid increase in accuracy and resolution of sensor payloads is the need to isolate that payload from the disturbances inherent to any spacecraft.

For single event upsets, the control problem lies in damping out vibrations incurred through the disturbance. Slew maneuvers, thruster firings, micro-meteorite collisions are all examples of SEU disturbances. Multiple event upsets, periodic or continuous disturbances, come in the form of high frequency vibrations from an internally mounted momentum wheel assembly, a cryogenic cooler apparatus, or any vibrating machinery that is part of the main spacecraft bus. The method of control for this type of disturbance is vibration isolation, and its control synthesis is inherently different from the damping control problem. In order for a precision sensor platform to be stable in the space environment and exhibit robustness in disturbance rejection, both types of control must be combined and used.

Optimal control is an excellent method to achieve both control specifications. For these types of applications, smart structures are a promising technology. In general, smart structures are the system elements that sense the dynamic state and change the

system's structural properties, such as its natural frequencies and its damping, to meet given performance objectives.

There are several types of embedded sensors and actuators which can be used for vibration and structural control. The embedded sensors are piezoelectric deformation sensors, strain gages, and fiber optic sensors. The embedded actuators are piezoceramic wafers, electrostrictive ceramic wafers, piezoceramic polymer film and shape memory metal wires. Piezoceramic sensors have a high strain sensitivity, a low noise baseline, low to moderate temperature sensitivity, and an ease of implementation. Piezoceramic actuators have high stiffness, sufficient stress to control vibration, good linearity, temperature insensitivity, are easy to implement, and minimize power consumption.

Conventional control methods have worked well in the past, but new design methods are required to obtain improved performance and robustness characteristics from the structural control system in order to satisfy future design specifications. Positive position feedback (PPF) and velocity feedback are two proven methods of structural control that work well with piezoceramic actuators and sensors. With a multiple-input-multiple-output (MIMO) control system, linear quadratic control methods are a preferred choice.

Linear quadratic control is based on full state feedback. If all the states are not known, an observer is inserted into the loop to estimate the unknown states. Linear quadratic controllers using state estimate feedback are optimal for the nominal plant models but the performance may be far from satisfactory in real life due to plant uncertainties, unmodeled plant dynamics, and sensor noise that is unaccounted for in the system compensator. Attractive passband robustness properties of full state feedback

optimal quadratic designs may disappear with the introduction of a state estimator. The Linear-Quadratic-Gaussian methodology provides an integrated frequency domain and state space approach for design of MIMO control systems. The advantages of the methodology lie in its ability to directly address design issues such as stability robustness and evaluate the trade-off between performance and allowable control authority.

II. SCOPE OF THESIS

The objective of this research is to achieve vibration suppression of a flexible antenna structure and also isolate vibration from the spacecraft main body. The flexible spacecraft simulator (FSS) in the Space Systems Dynamics and Control laboratory will be used to experimentally verify the data obtained from this analysis. The inherent spacecraft noise is in the form of vibrations from a continuous source, a momentum wheel mounted inside the spacecraft. The use of piezoceramic sensors and actuators to negate the disturbance vibration will be used. In addition, an external infrared optical sensor will be employed to provide structure position and velocity information to the optimal controller. The control technique we implement will be Optimal Linear Quadratic Gaussian (LQG) controller.

The approach will be to first characterize the flexible beam structure using finite element analysis and verify the results with elementary modal analysis. Using the modeshape information from this analytical model, optimum placement of the sensor/actuator pairs will be determined. Next is to construct an optimal control system using Linear Quadratic Regulator (LQR) optimal control with multiple sensors and actuators. Once the LQR control gains are satisfactory, an optimal observer will be added to the feedback path for smoothing and to estimate the unknown states plus filter out any high frequency noise.

The use of multiple sensors and actuators will enable the controller to quickly dampen out higher order modes of the reoccurring disturbance. Using SIMULINK, a vibration isolation system simulation will be designed, implemented and tested. The

optimal controller will be compared against known effective control schemes such as Positive Position Feedback (PPF) and derivative feedback control.

The follow on research will be to implement the LQG controller on the real time controller in the spacecraft dynamics and control laboratory, AC-100 from Integrated Systems, Inc.

III. CONTROL THEORY

A. BACKGROUND

State-space methods are the cornerstone of modern control theory. The essential difference between modern control theory and classical control theory is the characterization of a process by differential equations instead of transfer functions. In the modern approach, processes are represented by systems of coupled, first-order differential equations. In principle, there is no limit to the order of the system and in practice the limit is the availability of the computer software to perform the required calculations reliably.

B. STATE SPACE REPRESENTATION

Differential equations can be expressed as a set of simultaneous first-order differential equations. They are represented in state-variable form as the vector equations

$$\begin{aligned} \dot{\mathbf{x}} &= \mathbf{f}(\mathbf{x},\mathbf{u}) \\ \mathbf{y} &= \mathbf{h}(\mathbf{x},\mathbf{u}) \end{aligned} \tag{3.1}$$

where the input is **u**, and the output is **y**.

The column vector **x** is called the state of the system and contains n elements for a nth-order system. For mechanical systems, the states usually consist of the positions and velocities of the separate bodies. The vector function **f** relates the first derivative of the state to the state itself and the input u. Parameters in the function **f** could be dependent on time as well as position and velocity, but by and large, for structural systems the

parameters can be considered time-invariant. Linear approximations will be used for nonlinear systems in design and analysis. For the linear case, equation (3.1) can be written as

$$\begin{aligned} \dot{\mathbf{x}} &= \mathbf{A}\mathbf{x} + \mathbf{B}\mathbf{u} \\ \mathbf{y} &= \mathbf{C}\mathbf{x} + \mathbf{D}\mathbf{u} \end{aligned} \tag{3.2a,b}$$

where **A** is an $n \times n$ system matrix, **B** is an $n \times m$ control matrix, **C** is an $l \times n$ observer matrix and **D** is an $l \times m$ feed-through matrix(direct transmission matrix). Under most circumstances **D** is normally the zero matrix.

C. TRANSFORMATION OF STATE

For a system described by equations (3.2), that description is not a unique state description of the system. Matrix algebra enables a linear transformation of state without changing the basic properties of a matrix. Consider a state vector **z** where

$$\mathbf{x} = \mathbf{T}\mathbf{z} \tag{3.3}$$

and **T** is a nonsingular matrix. Substituting equation (3.3) into equation (3.2a), a linear transformation of state is performed

$$\dot{\mathbf{x}} = \mathbf{T}\dot{\mathbf{z}} = \mathbf{ATz} + \mathbf{Bu}$$
$$\dot{\mathbf{z}} = \mathbf{T}^{-1}\mathbf{ATz} + \mathbf{T}^{-1}\mathbf{Bu}$$
$$\dot{\mathbf{z}} = \mathbf{A}_T\mathbf{z} + \mathbf{B}_T\mathbf{u} \tag{3.4}$$

where

$$\mathbf{A}_T = \mathbf{T}^{-1}\mathbf{AT}$$
$$\mathbf{B}_T = \mathbf{T}^{-1}\mathbf{B}$$

Substituting equation (3.3) into equation (3.2b)

$$y = \mathbf{CTz} + \mathbf{Du}$$
$$= \mathbf{C}_T\mathbf{z} + \mathbf{Du} \tag{3.5}$$

where

$$\mathbf{C}_T = \mathbf{CT}$$

It is sometimes convenient to transform a physical system model into its *modal* canonical form, also known as the *Jordan* canonical form. This state description decouples the coupled first order equations into n independent first-order equations, providing that the system matrix is diagonalizable. This description has many advantages such as the degree of control authority the input has on each mode, the observability of each mode, and the damping ratio of each mode provided it is a damped system.

D. OPTIMAL CONTROL THEORY

An effective and widely used control technique of linear control systems is the optimal Linear Quadratic Regulator (LQR). Provided the full state vector is observable,

this method can be employed to fit specific design and performance criteria. A quadratic cost function, based on the Bolza problem, is used to minimize the performance index, *J*. The general form for the LQR is

$$J = \int (\mathbf{x}^T \mathbf{Q}\mathbf{x} + \mathbf{u}^T \mathbf{R}\mathbf{u}) dt \tag{3.6}$$

where **Q** is the state weighting matrix and **R** is the control weighting matrix. The necessary conditions for the optimal solution are that **Q** must be symmetric and positive semi-definite and **R** must be symmetric and positive definite. The solution to the LQR problem results in the optimum full state feedback gain matrix

$$\mathbf{K} = \mathbf{R}^{-1}\mathbf{B}'\mathbf{M} \tag{3.7}$$

where **M** satsfies the matrix Riccati equation

$$-\dot{\mathbf{M}} = \mathbf{M}\mathbf{A} + \mathbf{A}'\mathbf{M} - \mathbf{M}\mathbf{B}\mathbf{R}^{-1}\mathbf{B}'\mathbf{M} + \mathbf{Q} \tag{3.8a}$$

For a time-infinite solution, $\dot{\mathbf{M}}$ is set to zero. The control input is then

$$\mathbf{u} = -\mathbf{K}\mathbf{x} \tag{3.8b}$$

If the full state vector is not available, in order to use LQR control theory, it is necessary to design a state estimator or observer. The general form for an observer is given by

$$\dot{\hat{\mathbf{x}}} = \mathbf{A}\hat{\mathbf{x}} + \mathbf{B}\mathbf{u} + \mathbf{L}(y - \mathbf{C}\hat{\mathbf{x}}) \tag{3.9}$$

where $\hat{\mathbf{x}}$ is the estimated state vector. The inputs to the observer are the outputs from the plant and the control inputs to the plant.

By solving for the optimum observer gain, $\hat{\mathbf{L}}$, the observer is known as a Kalman filter. The general form of the dynamical equations used in the Kalman filter synthesis are

$$\begin{aligned} \dot{\mathbf{x}} &= \mathbf{A}\mathbf{x} + \mathbf{B}\mathbf{u} + \mathbf{F}v \\ y &= \mathbf{C}\mathbf{x} + \mathbf{D}\mathbf{u} + w \end{aligned} \tag{3.10}$$

where $\mathbf{F}$ is the plant uncertainty matrix, w is the state noise vector, and v is the sensor noise vector. Both v and w are considered to be white noise processes. White noise processes have the property of having a mean value of zero over time. This assumption does not always hold true in the real world but it simplifies the analysis considerably. The solution for the optimal observer gain is given by probability theory. The Kalman observer gain, $\hat{\mathbf{L}}$, is given by

$$\hat{\mathbf{L}} = \hat{\mathbf{P}}\mathbf{C}'\mathbf{W}^{-1} \tag{3.11}$$

where $\hat{\mathbf{P}}$ is taken from

$$\dot{\hat{\mathbf{P}}} = \mathbf{A}\hat{\mathbf{P}} + \hat{\mathbf{P}}\mathbf{A}' - \hat{\mathbf{P}}\mathbf{C}'\mathbf{W}^{-1}\mathbf{C}\hat{\mathbf{P}} + \mathbf{F}\mathbf{V}\mathbf{F}' \tag{3.12}$$

The process noise covariance matrices **V** and **W** are given by

$$\begin{aligned} E\{v(t)v'(t)\} &= \mathbf{V}(t)\delta(t-\tau) \\ E\{v(t)w'(t)\} &= \mathbf{X}(t)\delta(t-\tau) \\ E\{w(t)w'(t)\} &= \mathbf{W}(t)\delta(t-\tau) \end{aligned} \tag{3.13}$$

X(t) is the system cross-covariance matrix and is a function of the correlation of sensor noise to plant noise and under most circumstances it is normally zero. The symbol $E\{\ \}$ denotes mathematical expectation, in other words the average computed in the probabilistic sense.

E. CONTROLLABILITY AND OBSERVABILITY

Controllability and its dual, observability, are system parameters that indicate the extent that the states are controllable via the control matrix and for observability, the number of states that are observable via the sensors. They are two mutually independent functions of the system plant matrix, control matrix and the observer matrix. One simple test for controllability and observability is to form their respective matrices, the controllability matrix (**Mc**) and the observability matrix (**Mo**). Provided each matrix is of full rank, that indicates that the states are independent of one another and can be

controlled or observed. The degree of controllability or observability cannot be determined from this test; however converting the system to *Jordan* canonical form will indicate the relative control authority to the individual modal states and also the relative observability for each modal state.

The following are the equations for the respective matrices:

$$\mathbf{M}_c = \begin{bmatrix} \mathbf{B} & \mathbf{AB} & \mathbf{A}^2\mathbf{B} & \cdots & \mathbf{A}^{n-1}\mathbf{B} \end{bmatrix}$$

$$\mathbf{M}_o = \begin{bmatrix} \mathbf{C}^T & \mathbf{A}^T\mathbf{C}^T & (\mathbf{A}^T)^2\mathbf{C}^T & \cdots & (\mathbf{A}^T)^{n-1}\mathbf{C}^T \end{bmatrix}^T \tag{3.14}$$

A complete treatment is given in several textbooks, such as [Refs. 1,2]. These concepts will play a fundamental role in the design of the control system for the flexible structure. The whole concept of control design is a compromise between accuracy, complexity, and robustness. In particular, as this thesis will show, a very accurate model of the system might be not only too complex, but also it might be bound to be uncontrollable or unobservable. This is because an exact model is likely to contain a number of states, i.e., modes, which are hard to completely control with the given input signals. Likewise these same states might not be easily observable. When this is the case, the designer would look for a simpler model, where all the states are controllable and observable, and (hopefully) the effect of the neglected states will be within the noise level. For this problem the two matrices discussed above (controllability, observability) give a clear indication on the characteristics of the model.

IV. PIEZOELECTRIC THEORY

A. HISTORY OF PIEZOELECTRICITY

Piezoelectricity is a phenomenon that describes certain materials that generate electricity when a mechanical stress is applied, known as the direct effect, and also, that generate a mechanical stress when an electric field is applied on them. Piezoelectricity occurs naturally in some crystalline materials and can be induced in other polycrystalline materials through a process known as "poling". The material's crystal lattice structure may be poled by the application of a large electric field, usually at high temperature (see Fig. 4.1). [Ref. 3]

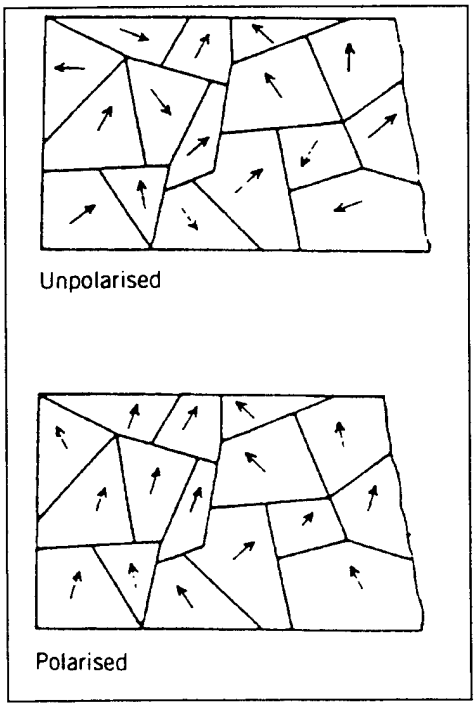

Figure 4.1. [Ref. 3] Crystalline Lattice Structures

Subsequent application of an electric field will produce additive strains locally which translate into a global strain for the material. The direct piezoelectric effect has been used for a long time in sensors such as accelerometers. Use of the converse effect, however, until recently has been restricted to ultrasonic transducers. Barium titanate, discovered in the 1940s, was the first widely used piezoceramic. Lead zirconate titanate (PZT), discovered in 1954 [Ref. 4], has now largely superseded barium titanate because of its stronger piezoelectric effects. Only recently have researchers in the area of structural control taken notice of the very desirable features of piezoelectric actuators and have started using them for many structural control applications. Piezoceramics are compact, have a very good frequency response and can be easily incorporated into structural systems. Actuation strains on the order of 1000 μstrain have been reported for PZT material. Strains are non-dimensional numbers which relate the change in length to the original length for a given impetus. Within the linear range they produce strains that are proportional to the applied electric field/voltage. These features make them very attractive for structural control applications.

There are several methods to model the constitutive behavior of piezoelectric materials. The most popular is the macromechanical approach, it provides the relationship between the electrical and mechanical effects in a manner that can be incorporated onto typical isotropic or orthotropic structural materials. For linear piezoelectric materials, the interaction between the electrical and mechanical variables can be described by linear relations of the form

$$S_i = s_{ij}^E T_j + d_{mi} E_m$$
$$D_m = d_{mi} T_i + \varepsilon_{mk}^T E_k \tag{4.1}$$

The mechanical variables are the stress T and the strain S, and the electrical variables are the electric field E and the electric displacement D; s is the compliance, d is the piezoelectric constant and ε is the permittivity. The first equation describes the converse piezoelectric effect, and the second equation describes the direct effect. The stress and strain are second order tensors, while the electric field and electric displacement are first order.

Figure 4.2 shows the typical coordinate system used to represent a poled piezoelectric. The 3-axis is in the direction of the initial polarization.

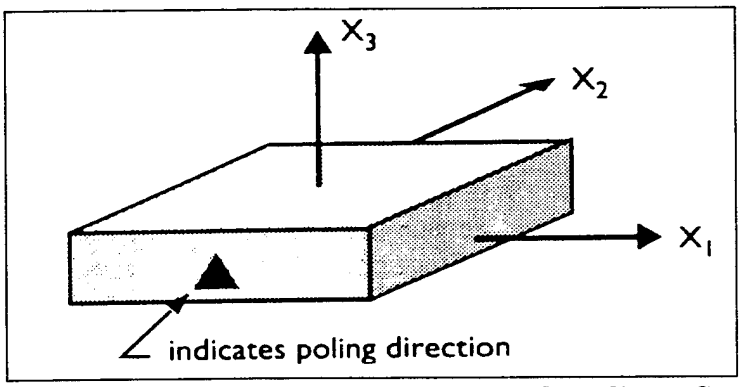

Figure 4.2. [Ref. 3] Typical Piezoceramic Coordinate System

The 1- and 2-axes are arbitrary in the plane perpendicular to the poling direction. The 1- and 2-axes are arbitrary because a poled piezoelectric is transversely isotropic in the 1–2 plane. The equations above written explicitly in matrix form are

$$\begin{bmatrix} S_1 \\ S_2 \\ S_3 \\ S_4 \\ S_5 \\ S_6 \\ D_1 \\ D_2 \\ D_3 \end{bmatrix} = \begin{bmatrix} s_{11}^E & s_{12}^E & s_{13}^E & 0 & 0 & 0 & 0 & 0 & d_{31} \\ s_{12}^E & s_{11}^E & s_{13}^E & 0 & 0 & 0 & 0 & 0 & d_{31} \\ s_{13}^E & s_{13}^E & s_{33}^E & 0 & 0 & 0 & 0 & 0 & d_{33} \\ 0 & 0 & 0 & s_{55}^E & 0 & 0 & 0 & d_{15} & 0 \\ 0 & 0 & 0 & 0 & s_{55}^E & 0 & d_{15} & 0 & 0 \\ 0 & 0 & 0 & 0 & 0 & s_{66}^E & 0 & 0 & 0 \\ 0 & 0 & 0 & 0 & d_{15} & 0 & \varepsilon_1^T & 0 & 0 \\ 0 & 0 & 0 & d_{15} & 0 & 0 & 0 & \varepsilon_1^T & 0 \\ d_{31} & d_{31} & d_{33} & 0 & 0 & 0 & 0 & 0 & \varepsilon_3^T \end{bmatrix} \begin{bmatrix} T_1 \\ T_2 \\ T_3 \\ T_4 \\ T_5 \\ T_6 \\ E_1 \\ E_2 \\ E_3 \end{bmatrix} \tag{4.2}$$

Where S_1 through S_3 are the normal strains, S_4 through S_6 are the shear strains, T_1 through T_3 are the normal stresses, T_4 through T_6 are the shear stresses, D_1 through D_3 are the electric displacements and E_1 through E_3 are the electric fields associated with the given coordinate system.

The piezoelectric constants that are of most interest from a structural standpoint are the *d* constants. These constants relate the strain developed in the material to the applied electric field; obviously, the highest value of these constants is desirable. The d_{33} constant relates the strain in the 3-direction to the field in the 3-direction.; similarly, the d_{31} relates the strain in the 1-direction to the electric field in the 3-direction. The electric field is voltage applied across the piezoelectric divided by its thickness. It is important to point out that d_{33} is usually a positive number and d_{31} is a negative number. This means that a positive field (i.e., a field applied in the poling direction) will produce a positive mechanical strain in the 3-direction and a negative strain in the 1-direction.

There are many applications for the use of PZT actuators and they can be divided into two general categories: the linear actuators and the actuators used for structural

control applications. In the first category, the PZT actuators, arranged in the form of stacks, are used in a fashion similar to shakers or conventional hydraulic or electrical actuators. Due to the fact that the stroke is severely limited, in static applications they are used only for micropositioning work. In structural control applications, the actuators are typically embedded or bonded to the surfaces of the structure and they apply localized strains that can be used directly to control structural deformations. A typical arrangement is shown in Figure 4.3; the two actuators are on the upper and lower surfaces of the structure and are actuated out of phase (the upper expands and the lower contracts), which creates a moment on the structure. [Ref. 3]

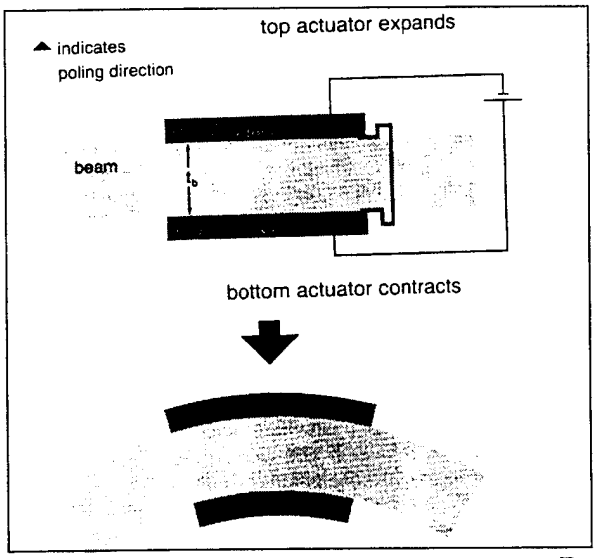

Figure 4.3. [Ref. 3] Piezoceramic Actuator Pair

In the remainder of this chapter we will apply piezoceramic actuators and sensors as structural control elements.

B. FLEXIBLE SPACECRAFT SIMULATOR PIEZOCERAMIC ACTUATORS AND SENSORS.

Piezoceramic sensors and actuators are located on the flexible appendage as shown in Figure 4.4. The piezoceramic wafers are bonded to the surface of the flexible arm and the voltage developed from the sensors is fed to the actuators by way of the designed control system.

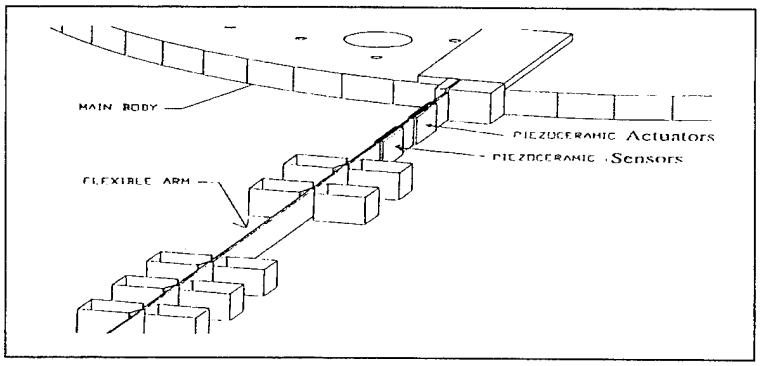

Figure 4.4. Piezoceramic Actuators and Sensors Mounted on the FSS Flexible Beam

Figure 4.5 illustrates the orientation of a piezoceramic wafer on an arm and the alignment of its axis that describes the electro-mechanical relationships.

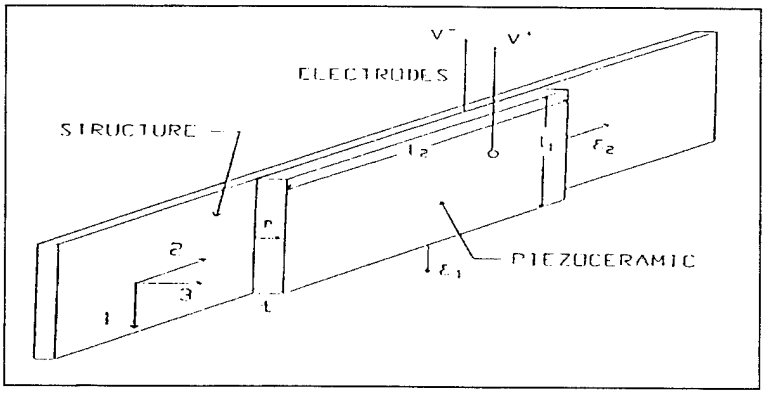

Figure 4.5. Poled Piezoceramic Mounted on FSS Beam

The piezoceramic wafers in a sensory mode produce a charge between their electrodes that is directly proportional to the lateral strains. It is given by

$$Q = AEd_{31}(\varepsilon_1 + \varepsilon_2) \tag{4.3}$$

where A is the lateral area of the piezoceramic wafer, E is Young's modulus of the wafer, d_{31} is the lateral charge coefficient, and ε_1 and ε_2 are the strain values in the lateral directions respectively. The capacitance for a piezoceramic wafer as shown in Figure 4.5 is given by

$$C = \frac{DA}{t} \tag{4.4}$$

where D is the dielectric constant of the piezoceramic and t is the thickness of the wafer. The voltage V produced by a sensor under strain is given by

$$V = \frac{Q}{C} = \frac{Ed_{31}}{D} t(\varepsilon_1 + \varepsilon_2) \tag{4.5}$$

When using piezoceramic wafers as actuators, the attachment geometry is similar to the sensor geometry shown in Figure 4.5. The control voltage , e_c, is applied to the wafers and the lateral strain that is developed can act to control the bending of the beam. The electric field that is developed by the wafer is given by

$$\Phi = \frac{VC}{t_p} \tag{4.6}$$

Care must be taken not to induce a strong electric field that is opposed to the piezoceramic's poling direction as that can damage the material by depolarizing it. Typical field limits by most materials are between 500 and 1000 volts/mm.

Table 4.1 is a good reference for the material properties of piezoceramics. For this thesis, Navy Type II PZT piezoceramic element is used, which is material EC-66 in Table 4.1. It is a above average piezoceramic material which boasts an excellent Lateral Strain coefficient (d_{31}) and exhibits good linearity properties between applied voltages of ±150 volts.

Table 4.1. [Ref. 3] Piezoelectric Materials and Properties.

Electromechanical Properties:	Barium Titanate				Lead Zirconate Titanate								Lead Titanate	Lead Magnesium Niobate
	EC-21	EC-31	EC-55	EC-57	EC-63	EC-64	EC-65	EC-66	EC-67	EC-69	EC-70	EC-76	EC-97	EC-98
Physical properties														
Density ($\times 10^3$ kg/m^3)	5.7	5.55	5.55	5.3	7.5	7.5	7.5	7.45	7.5	7.5	7.45	7.45	6.7	7.85
Young's modulus ($\times 10^{10}$ N/m^2)	11.4	10.7	11.6	12.5	8.9	7.8	6.6	6.2	9.3	9.9	6.3	6.4	12.8	6.1
Curie temperature (°C)	130	115	115	140	320	320	350	270	300	300	220	190	240	170
Mechanical Q for a thin disk	1400	400	550	600	500	400	100	80	900	960	75	65	950	70
Electric properties at 25°C														
Dielectric constant at 1 kHz	1070	1170	1220	640	1250	1300	1725	2125	1100	1050	2750	3450	270	5500
Dissipation constant at 1 kHz low field	0.5	0.7	0.5	0.6	0.4	0.4	2.0	2.0	0.3	0.3	2.0	2.0	0.9	2.0
K_{31}	0.17	0.19	0.19	0.15	0.34	0.35	0.36	0.36	0.33	0.31	0.37	0.38	0.01	0.35
K_p	0.26	0.32	0.31	0.25	0.58	0.60	0.62	0.62	0.56	0.52	0.63	0.64	0.01	0.61
K_{33}	0.38	0.48	0.46	0.38	0.68	0.71	0.72	0.72	0.66	0.62	0.74	0.75	0.53	0.72
K_{15}	0.37	0.49	0.48	0.23	0.69	0.72	0.69	0.68	0.59	0.55	0.67	0.68	0.35	0.67
d_{31} ($\times 10^{-12}$ m/V)	−49	−59	−58	−32	−120	−127	−173	−198	−107	−95	−230	−262	−3	−312
d_{33} ($\times 10^{-12}$ m/V)	117	152	150	87	270	295	380	415	241	220	490	583	68	730
d_{15} ($\times 10^{-12}$ m/V)	191	248	245	154	475	506	584	626	362	330	670	730	67	825
g_{31} ($\times 10^{-3}$ V·m/N)	−5.2	−5.8	−5.6	−5.5	−10.3	−10.7	−11.5	−10.6	−10.9	−10.2	−9.8	−8.6	−1.7	−6.4
g_{33} ($\times 10^{-3}$ V·m/N)	12.4	14.8	14.3	16.2	24.1	25.0	25.0	23.0	24.8	23.7	20.9	19.1	32.0	15.6
g_{15} ($\times 10^{-3}$ V·m/N)	15.7	20.4	20.1	28.0	37.0	39.8	38.2	36.6	28.7	28.9	35.0	28.9	33.5	17.0
Elastic constant														
S_{11}^E ($\times 10^{-12}$ m^2/n)	8.8	9.3	8.6	8.0	11.3	12.8	15.2	16.1	10.8	10.1	15.9	15.6	—	16.3
S_{12}^E ($\times 10^{-12}$ m^2/n)	−2.7	−2.9	−2.6	−2.2	−3.7	−4.2	−5.3	−5.5	−3.6	−3.4	−5.4	−4.7	—	−5.6
S_{33}^E ($\times 10^{-12}$ m^2/n)	10.0	9.7	9.8	9.3	14.3	15.0	18.3	17.7	13.7	13.5	18.0	19.8	7.7	21.1
Aging rate (% change per time decade)														
Dielectric constant	−4.5	−1.8	−1.6	−4.8	−4.1	−4.2	−0.8	−1.5	−3.2	−3.0	−2.1	−2.0	−0.3	−1.5
Coupling constant	−4.0	−2.0	−1.4	−5.0	−2.1	−2.1	−0.3	−0.4	−1.6	−1.4	−0.4	−0.4	−0.4	−0.4
Resonant frequency	0.85	0.4	0.6	0.8	1.0	1.0	0.2	0.3	0.8	0.75	0.4	0.3	0.05	0.4
Electric field dependence														
rms kV/m at 25°C	79	79	79	79	394	394	79	79	394	394	79	79	79	79
Dielectric constant (% increase)	1.4	6.0	3.0	0.4	18.0	18.0	12.0	12.3	3.8	3.2	12.6	14.0	1.5	22.5
Dissipation factor (%)	0.7	4.0	0.9	0.7	3.0	3.0	7.3	6.9	0.9	0.6	7.1	7.9	0.8	6.2

[a]Values are nominal; actual production values vary ± 10%.

Source: EDO Corporation (2), **compliments of the EDO Corporation**

V. FINITE ELEMENT ANALYSIS

A. BACKGROUND

The need for characterization of complex structures and the advent of the modern day computer has given rise to a method of analysis known as the finite element method. The idea behind the finite element method is to provide a formulation which can exploit digital computer automation for the analysis of irregular systems. To this end the method regards a complex structure as an assemblage of finite elements, which every such element is part of a continuous structural member. By requiring that the displacements be compatible and the internal forces in balance at certain points shared by several elements, where the points are known as nodes, the entire structure is compelled to act as one entity.

The finite element method of analysis, while considering a continuous structure, is a discretization problem in that it expresses the displacements of the continuous structure in terms of a finite number of displacements at the nodal points multiplied by the interpolation functions. The advantage of the finite element method over any other method is that the equations for the system can be derived by first deriving the equations for a single element and then assembling the individual elements' equations by using constraint conditions. The displacement at any point inside the element is obtained by means of interpolation, where the interpolation functions are generally low-degree polynomials and they are the same for every element. [Ref. 5]

B. ELEMENT STIFFNESS MATRIX

Meirovitch [Ref. 5, pp. 303-304] uses the direct method for derivation of the elemental stiffness matrix. The stiffness matrix relates a displacement vector to a force vector. Using the element in Figure 5.1, for uniform bending stiffness, the differential equation for the displacement *w(x)* is

$$EI\frac{d^4w(x)}{dx^4} = 0 \qquad 0 < x < h \tag{5.1}$$

where E is Young's modulus for the material and I is the area moment of inertia for the beam cross-section.

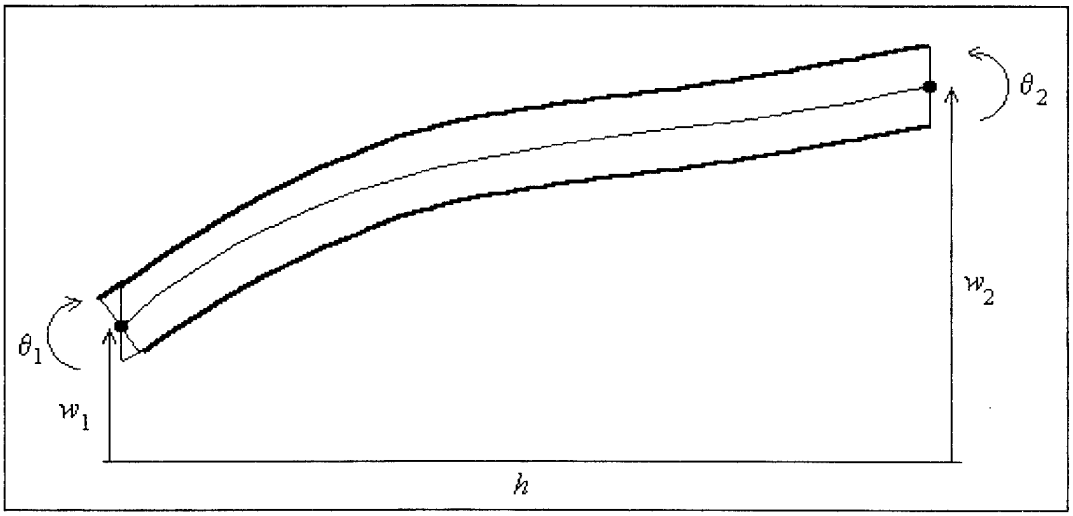

Figure 5.1. Beam Element for Finite Element Model

By integrating four times, we have the elemental displacement at any point

$$w(x) = \tfrac{1}{6}c_1x^3 + \tfrac{1}{2}c_2x^2 + c_3x + c_4 \tag{5.2}$$

with c_1 through c_4 as the constants of integration, determined from the boundary conditions

$$w(0) = w_1 \qquad \left.\frac{dw(x)}{dx}\right|_{x=0} = \theta_1 \qquad w(h) = w_2 \qquad \left.\frac{dw(x)}{dx}\right|_{x=h} = \theta_2 \tag{5.3}$$

w_1 and w_2 are the nodal displacements and θ_1 and θ_2 are the nodal rotations at the endpoints of the element. By solving equation (5.2) into (5.3) the corresponding constants of integration are solved as

$$c_1 = \frac{6}{h^3}(2w_1 + h\theta_1 - 2w_2 + h\theta_2) \qquad c_2 = \frac{2}{h^2}(-3w_1 - 2h\theta_1 + 3w_2 - h\theta_2)$$

$$c_3 = \theta_1 \qquad c_4 = w_1 \tag{5.4}$$

Hence, introducing equation (5.4) into (5.2), the expression for the bending displacement is determined to be

$$w(x)=\left[1-3\left(\frac{x}{h}\right)^2+2\left(\frac{x}{h}\right)^3\right]w_1+\left[\frac{x}{h}-2\left(\frac{x}{h}\right)^2+\left(\frac{x}{h}\right)^3\right]h\theta_1 +\left[3\left(\frac{x}{h}\right)^2-2\left(\frac{x}{h}\right)^3\right]w_2+\left[-\left(\frac{x}{h}\right)^2+\left(\frac{x}{h}\right)^3\right]h\theta_2 \tag{5.5}$$

The bending displacement is related to the inter-element nodal forces f_1,$f2$, $f3$, and $f4$ as follows

$$EI\frac{d^3w(x)}{dx^3}\bigg|_{x=0}=f_1 \qquad EI\frac{d^2w(x)}{dx^2}\bigg|_{x=0}=-f_2$$
$$EI\frac{d^3w(x)}{dx^3}\bigg|_{x=h}=-f_3 \qquad EI\frac{d^3w(x)}{dx^3}\bigg|_{x=h}=f_4 \tag{5.6}$$

Combining equations (5.6) and (5.5) yields

$$\begin{aligned} f_1 &= \frac{EI}{h^3}(12w_1+6h\theta_1-12w_2+6h\theta_2)\\ f_2 &= \frac{EI}{h^2}(6w_1+4h\theta_1-6w_2+2h\theta_2)\\ f_3 &= \frac{EI}{h^3}(-12w_1-6h\theta_1+12w_2-6h\theta_2)\\ f_4 &= \frac{EI}{h^2}(6w_1+2h\theta_1-6w_2+4h\theta_2) \end{aligned} \tag{5.7}$$

This can be written in matrix form as

$$[k]\{q\}=\{f\} \tag{5.8}$$

where the nodal displacement vector and the nodal force vector are given by

$$\{q\} = \begin{Bmatrix} w_1 \\ \theta_1 \\ w_2 \\ \theta_2 \end{Bmatrix} \qquad \{f\} = \begin{Bmatrix} f_1 \\ f_2 \\ f_3 \\ f_4 \end{Bmatrix} \tag{5.9}$$

and the element stiffness matrix is given by

$$[k] = \frac{EI}{h^3}\begin{bmatrix} 12 & 6h & -12 & 6h \\ 6h & 4h^2 & -6h & 2h^2 \\ -12 & -6h & 12 & -6h \\ 6h & 2h^2 & -6h & 4h^2 \end{bmatrix} \tag{5.10}$$

C. ELEMENT MASS MATRIX

Equation (5.5) can be written as a function of the nodal displacements and interpolation functions, *L(x)*

$$w(x) = L_1(x)w_1 + L_2(x)h\theta_1 + L_3(x)w_2 + L_4(x)h\theta_2 \tag{5.11}$$

where

$$\begin{aligned} L_1(x) &= \left[1 - 3\left(\frac{x}{h}\right)^2 + 2\left(\frac{x}{h}\right)^3\right] & L_3(x) &= \left[3\left(\frac{x}{h}\right)^2 - 2\left(\frac{x}{h}\right)^3\right] \\ L_2(x) &= \left[\frac{x}{h} - 2\left(\frac{x}{h}\right)^2 + \left(\frac{x}{h}\right)^3\right] & L_4(x) &= \left[-\left(\frac{x}{h}\right)^2 + \left(\frac{x}{h}\right)^3\right] \end{aligned} \tag{5.12}$$

Equations (5.11) and (5.12) can be expressed in matrix form

$$w(x,t) = \{L(x)\}^T \{x(t)\} \tag{5.13}$$

with $\{L(x)\}$ as a four-dimensional vector of the interpolation functions and $\{x(t)\}$ a four-dimensional vector of nodal displacements. The element kinetic energy has the form

$$T(t) = \frac{1}{2}\int_0^h m(x)\left[\frac{\partial^2 w(x,t)}{\partial t^2}\right]^2 dx = \tfrac{1}{2}\{\dot{w}(t)\}^T [m]\{\dot{w}(t)\} \tag{5.14}$$

where the 4×4 mass matrix is given by

$$[m] = \int_0^h m(x)\{L(x)\}\{L(x)\}^T dx \tag{5.15}$$

Inserting the interpolation functions vector, equation (5.12), into equation (5.15) and integrating over the element length, the elemental mass matrix becomes

$$[m] = \frac{mh}{420}\begin{bmatrix} 156 & 22h & 54 & -13h \\ 22h & 4h^2 & 13h & -3h^2 \\ 54 & 13h & 156 & -22h \\ -13h & -3h^2 & -22h & 4h^2 \end{bmatrix} \tag{5.16}$$

D. ASSEMBLING THE GLOBAL MASS AND STIFFNESS MATRICES INTO THE COMPLETE SYSTEM

The next step is to assemble each element's mass and stiffness matrices into the global system mass matrix and the system global stiffness matrix, respectively. The assembling procedure is an algebraic process of adding the overlapping element matrices together. Consider the 4×4 element matrix partitioned into a 2×2 matrix of 2×2 sub-matrices

$$[m^1] = \begin{bmatrix} m^1{}_{11} & m_{12}{}^1 \\ m^1{}_{21} & m^1{}_{22} \end{bmatrix} \quad [m^2] = \begin{bmatrix} m^2{}_{11} & m^2{}_{12} \\ m^2{}_{21} & m^2{}_{22} \end{bmatrix} \quad \cdots \quad [m^n] = \begin{bmatrix} m^n{}_{11} & m^n{}_{12} \\ m^n{}_{21} & m^n{}_{22} \end{bmatrix} \tag{5.17}$$

The global system matrix is required to be symmetric and is constructed by adding the element matrices along the diagonal

$$[M] = \sum_{1}^{n} [m^n] \tag{5.18}$$

For example, with three elements this matrix becomes

$$[M] = \begin{bmatrix} m_{11}^{1} & m_{12}^{1} & 0 & 0 \\ m_{21}^{1} & m_{22}^{1} + m_{11}^{2} & m_{12}^{2} & 0 \\ 0 & m_{21}^{2} & m_{22}^{2} + m_{11}^{3} & m_{12}^{3} \\ 0 & 0 & m_{21}^{3} & \ddots \end{bmatrix} \tag{5.19}$$

The method is the same for both the stiffness and the mass matrices. In order to satisfy the boundary conditions for a fixed-free system, the displacement and rotation at the root of the flexible appendage must be zero. This condition is satisfied by eliminating the first and second rows and the first and second columns from both the global mass and stiffness matrices, respectively.

E. PIEZOELECTRIC FINITE ELEMENT MODELING

The piezoceramic elements used in the structure must be incorporated into the finite element model. The basic equations for both piezoceramic actuators and sensors are the same as for ordinary structural elements discussed in the previous section. There is a need to compensate for the piezoceramic displacement from the center of the beam and Figure 5.2 illustrates this concept. In addition, the electro-mechanical relationships must be taken into account for implementation into an analytical model suitable for control design.

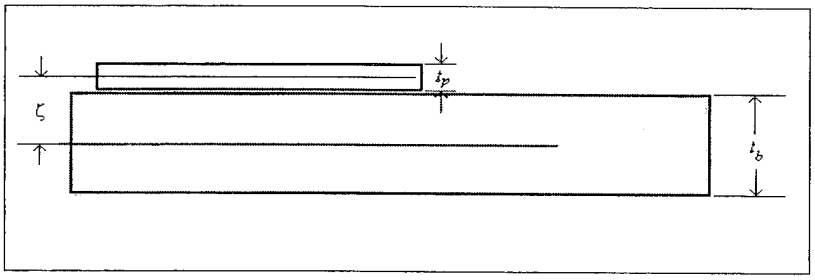

Figure 5.2. Piezoceramic Element Placement on Beam

From equation (4.1) the general relationship for the electro-mechanical coupling is given by

$$\begin{Bmatrix} D_3 \\ S_1 \end{Bmatrix} = \begin{bmatrix} \varepsilon_3^T & d_{31} \\ d_{31} & s_{11}^E \end{bmatrix} \begin{Bmatrix} E_3 \\ T_1 \end{Bmatrix} \tag{5.20}$$

Using the fact that the elastic constant for piezoceramic material, s, is the inverse of its Young's modulus, E_p, this equation can be written as

$$\begin{Bmatrix} D_3 \\ T_1 \end{Bmatrix} = \begin{bmatrix} \varepsilon_3^T - d_{31}{}^2 E_p & d_{31} E_p \\ -d_{31} E_p & E_p \end{bmatrix} \begin{Bmatrix} E_3 \\ S_1 \end{Bmatrix} \tag{5.21}$$

The next step is to set up the equation for the elemental potential energy, U.

$$-U = \frac{1}{2} \int_V (-T_1 S_1 + D_3 E_3) dV \tag{5.22}$$

where the two terms in the integral represent mechanical energy ($T_1 S_1$) and electrical energy ($D_3 E_3$). Using w_p as the width of the piezoceramic wafer, this equation can be rewritten as

$$\begin{aligned} -U &= \frac{1}{2} w_p \int_0^h \int_\zeta^{\zeta + t_p} (-T_1 S_1 + D_3 E_3) dx dz \\ &= \frac{1}{2} w_p \int_0^h \int_\zeta^{\zeta + t_p} \begin{Bmatrix} D_3 \\ T_1 \end{Bmatrix}^T \begin{bmatrix} 1 & 0 \\ 0 & -1 \end{bmatrix} \begin{Bmatrix} E_3 \\ S_1 \end{Bmatrix} dx dz \end{aligned} \tag{5.23}$$

The strain, using small angle displacement theory, S_1, can be written as

$$S_1 = \varepsilon_x = -z\frac{\partial^2 w}{\partial x^2} \tag{5.24}$$

substituting equation (5.21) into equation (5.23)

$$\begin{aligned} -U &= \frac{1}{2} w_p \int_0^h \int_\zeta^{\zeta+t_p} \begin{Bmatrix} E_3 \\ \varepsilon_x \end{Bmatrix}^T \begin{bmatrix} \varepsilon_3^T - d_{31}{}^2 E_p & d_{31} E_p \\ d_{31} E_p & -E_p \end{bmatrix} \begin{Bmatrix} E_3 \\ \varepsilon_x \end{Bmatrix} dxdz \\ &= \frac{1}{2} w_p \int_0^h \int_\zeta^{\zeta+t_p} \left[(\varepsilon_3^T - d_{31}{}^2 E_p) E_3{}^2 + 2 d_{31} E_p E_3 \varepsilon_x - E_p \varepsilon_x{}^2 \right] dxdz \end{aligned} \tag{5.25}$$

then, using equation (5.24)

$$-U = \frac{1}{2} w_p \int_0^h \int_\zeta^{\zeta+t_p} \left[(\varepsilon_3^T - d_{31}{}^2 E_p) E_3{}^2 + 2 d_{31} E_p E_3 z \frac{\partial^2 w}{\partial x^2} - E_p z^2 \left(\frac{\partial^2 w}{\partial x^2} \right)^2 \right] dxdz \tag{5.26}$$

Rewriting equation (5.13) in terms of a summation

$$w(x,t) = \sum_{i=1}^{4} \Phi_i(x) q_i(t) \tag{5.27}$$

where Φ is the vector of interpolation functions or "modeshapes" and q is the nodal vector from equation (5.9a). Inserting this equation along with the interpolation functions, equation (5.12), the general form of the energy equation is

$$-U = \frac{1}{2}\gamma e^2 - q^T be - \frac{1}{2} q^T k_p q$$

where

(5.28)

$$\gamma = \frac{w_p h}{t_p}\left(\varepsilon_3^T - {d_{31}}^2 E_p\right), \quad e = t_p E_3$$

$$b_i = d_{31} E_p w_p \left(\zeta + \frac{t_p}{2}\right) \int_0^h \frac{d^2\Phi_i(x)}{dx^2} dx$$

$$\left[k_p\right]_{ij} = w_p E_p t_p \left[\zeta^2 + \zeta t_p + \frac{{t_p}^2}{3}\right] \int \frac{d^2\Phi_i(x)}{dx^2} \frac{d^2\Phi_j(x)}{dx^2} dx$$

Substituting the interpolation functions from equation (5.12) into the b vector, we get

$$\begin{aligned} b_1 &= 0 \\ b_2 &= -d_{31} E_p w_p \left(\zeta + \frac{t_p}{2}\right) \\ b_3 &= 0 \\ b_4 &= d_{31} E_p w_p \left(\zeta + \frac{t_p}{2}\right) \end{aligned} \qquad (5.29)$$

and into the piezoceramic elemental stiffness matrix, $[k_p]$

$$[k_p] = \frac{\kappa}{h}\begin{bmatrix} \frac{12}{h^2} & \frac{6}{h} & -\frac{12}{h^2} & \frac{6}{h} \\ \frac{6}{h} & 4 & -\frac{6}{h} & 2 \\ -\frac{12}{h^2} & -\frac{6}{h} & \frac{12}{h^2} & -\frac{6}{h} \\ \frac{6}{h} & 2 & -\frac{6}{h} & 4 \end{bmatrix}$$

$$\kappa = w_p t_p E_p (\zeta^2 + \zeta t_p + \frac{t_p^2}{3}) \tag{5.30}$$

The piezoceramic elemental mass matrix is derived in the same fashion as an ordinary structural element with the exception that the piezoceramic material linear mass density be used instead of the ordinary material density of the structure to which it is bonded.

For structural elements that have piezoceramic material bonded to them, their respective mass and stiffness matrices are given by the simple addition of the beam elemental matrices and the piezoceramic elemental matrices which are then assembled into global mass and stiffness matrices as in the previous section.

$$[M]_{element} = [m]_{beam} + [m]_{piezo}$$
$$[K]_{element} = [k]_{beam} + [k]_{piezo} \tag{5.31}$$

VI. ANALYTICAL MODEL

A. FLEXIBLE SPACECRAFT SIMULATOR ARM

The Spacecraft Dynamics and Control Laboratory Flexible Spacecraft Simulator (FSS) simulates attitude motion about the pitch axis of a spacecraft. As shown in Figure 6.1 it consists of a single degree-of-freedom rigid central body, representing the spacecraft central body, and a multiple degree-of-freedom flexible appendage, representing an antenna reflector with a flexible support structure.

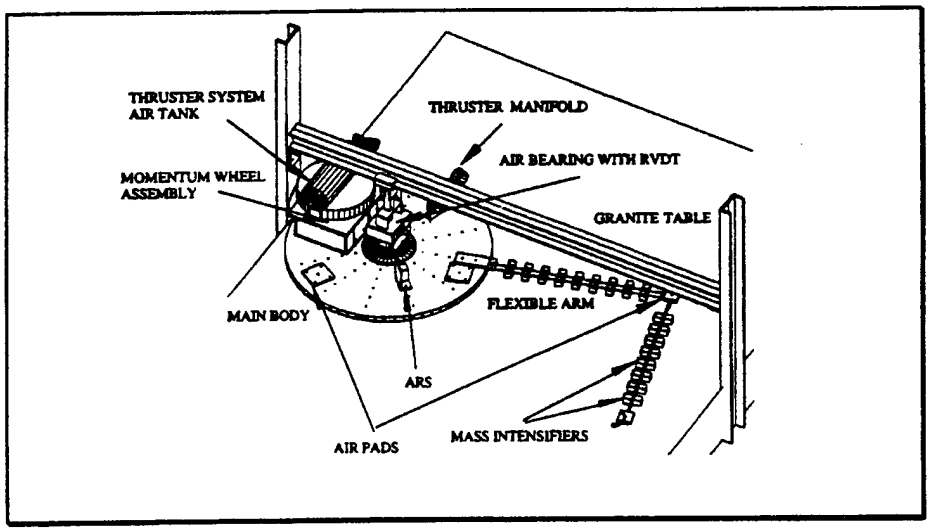

Figure 6.1. NPS Flexible Spacecraft Simulator (FSS)

Piezoceramic sensors and actuators are used to provide active damping to the flexible support structure. The entire system is floated on air pads over a finely ground granite table to simulate a microgravity environment. The central body has two thrusters and a momentum wheel as its actuators. The flexible appendage has two stacked piezoceramic pairs as actuators. The first pair is located at the base of the arm assembly

and the second is located at the base of the forearm near the structure's elbow as in Figure 6.2.

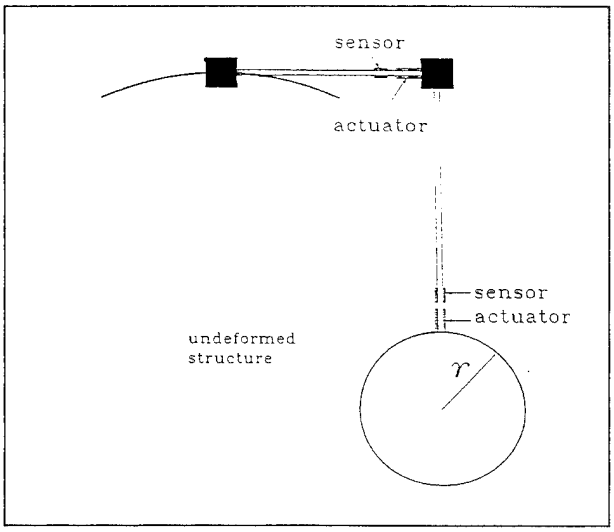

Figure 6.2. FSS Experimental Setup for LQG/Vision Server Testing

A finite element model will be used to simulate the flexible appendage. The elemental mass and stiffness matrices are given by equations (5.16) and (5.10), respectively. Using equation (5.18) to assemble both the global mass matrix, **M**, and global stiffness matrix, **K**, and by the use of Newtonian physics, the equations of motion can be derived. Figure 6.3 reveals the finite element model used for this research.

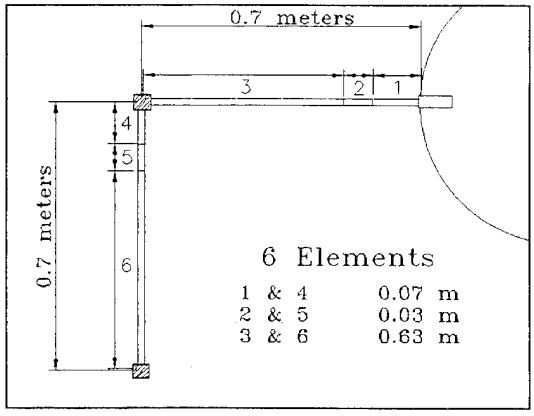

Figure 6.3. Finite Element Model of the FSS Flexible Appendage

Table 6.1 gives the material properties and parameters used on this model.

7075 T-6 Aluminum Beam			
Quantity	**Description**	**Units**	**Value**
t_b	Beam thickness	meters	1.5875×10^{-3}
w_b	Beam width	meters	0.0254
ρ_b	Beam density	kg/m^3	2800
E_b	Young's Modulus	N/m^2	1.029×10^7
Navy Type II PZT			
Quantity	**Description**	**Units**	**Value**
d_{31}	Lateral strain coefficient	*m/V* or *Coul/N*	-1.8×10^{-10}
E_p	Young's Modulus	N/m^2	6.3×10^{10}
ν	Poisson's ratio	N/A	0.35
D	Absolute permittivity	*Farad/m* or N/V^2	1.5×10^{-8}

Table 6.1. Model Material Properties

B. EQUATIONS OF MOTION

In this section we derive the equations of motion for a twelve degree-of-freedom dynamic model. The derivation goes along the lines of a two-degree-of-freedom system as shown in Figure 6.4.

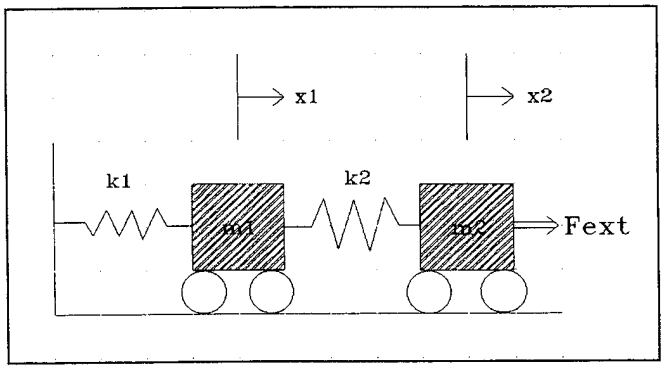

Figure 6.4. Two Degree-of-freedom Model

From Newton's Law

$$\sum \mathbf{F} = m\mathbf{a} \tag{6.1}$$

applied to each mass we obtain

$$m_1\ddot{x}_1 = -k_1x_1 + k_2(x_2 - x_1) \qquad m_2\ddot{x}_2 = -k_2(x_2 - x_1) + F \tag{6.2}$$

Using a vector $\mathbf{x} = \begin{Bmatrix} x_1 \\ x_2 \end{Bmatrix}$, and grouping like terms

$$\begin{bmatrix} m_1 & 0 \\ 0 & m_2 \end{bmatrix} \begin{Bmatrix} \ddot{x}_1 \\ \ddot{x}_2 \end{Bmatrix} + \begin{bmatrix} k_1 + k_2 & -k_2 \\ -k_2 & k_2 \end{bmatrix} \begin{Bmatrix} x_1 \\ x_2 \end{Bmatrix} = \begin{Bmatrix} 0 \\ 1 \end{Bmatrix} F \tag{6.3}$$

or $$\mathbf{M}\ddot{\mathbf{x}} + \mathbf{K}\mathbf{x} = \mathbf{F}$$

where **M** is the mass matrix, **K** is the stiffness matrix, and **F** is the force vector.

This type of dynamic representation relates directly to finite element analysis with appropriate modifications to account for piezoceramic sensors and actuators in the finite element model.

Using the principle of virtual work and using the Lagrangian method of analysis, the kinetic energy for a piezoceramic element can be written as

$$T = \frac{1}{2}\int_0^h \rho_p \dot{w}^2 dx \tag{6.4}$$

where ρ_p is the mass per unit length for the piezoceramic and $\dot{w}$ is the velocity at any point on the element. An alternative form of equation (6.4) is

$$T = \frac{1}{2}\dot{\mathbf{q}}^T \mathbf{m}_p \dot{\mathbf{q}} \tag{6.5}$$

where

$$\left[\mathbf{m}_p\right]_{ij} = \int_0^h \rho_p \phi_i(x)\phi_j(x)dx \tag{6.6}$$

given ϕ the interpolation functions from equation (5.12). The total kinetic energy for a beam mounted piezoceramic is then

$$T = \frac{1}{2}\dot{\mathbf{q}}^T \mathbf{M}\dot{\mathbf{q}} \tag{6.7}$$

where the mass matrix is given by equation (5.31).

The Lagrangian function, L, is given by

$$L = T - U$$

$$= \frac{1}{2}\dot{\mathbf{q}}^T\mathbf{M}\dot{\mathbf{q}} + \frac{1}{2}\gamma e_a^{\,2} - \mathbf{q}^T\mathbf{B}e_a - \frac{1}{2}\mathbf{q}^T\mathbf{K}\mathbf{q} \tag{6.8}$$

which is used in the equations of motion

$$\frac{d}{dt}\left(\frac{\partial L}{\partial \dot{\mathbf{q}}_k}\right) - \frac{\partial L}{\partial \mathbf{q}_k} = 0 \tag{6.9}$$

Substituting equation (6.8) into (6.9) and using $\mathbf{q}$ as generalized coordinates the actuator equation becomes

$$\mathbf{M}\ddot{\mathbf{q}} + \mathbf{K}\mathbf{q} = -\mathbf{B}e_a \tag{6.10}$$

where $\mathbf{B}$ comes from equation (5.29) and e_a is the applied voltage to the piezoceramic element. This is the modified version of equation (6.3) that must be used for the dynamical system model.

If the voltage e is taken in terms of generalized coordinates, the equation in terms of voltage is

$$e = \frac{1}{\gamma}\mathbf{B}^T\mathbf{q} \tag{6.11}$$

Equation (6.11) represents the voltage output from a piezoceramic sensor.

Using the material properties from Table 6.1 and the preceding equations of motion, the finite element model produced twelve natural modes of vibration. Appendix A contains the MATLAB script file, **fem.m**, that was used to solve this model. Table 6.2 gives the values for the natural frequencies and Figures 6.5 and 6.6 give the modeshapes for the first two modes. Appendix B contains the graphs for all twelve modeshapes. These two modes are the primary carriers of energy for the structure and it is they that the compensator will be designed to actively control.

Mode	Frequency (Hz)
1	**0. 2958**
2	**0.8707**
3	11.108
4	28.496
5	45.144
6	102.78
7	278.83
8	341.04
9	1347.7
10	1392.7
11	5284.5
12	5343.0

Table 6.2. Finite Element Model Natural Frequencies

Convergence of a finite element model to its analytical counterpart is dependent on the number of elements used in the model, the higher the number of elements the quicker the model is to converge to the actual values. A finite element model's accuracy can be roughly estimated as half the number of elements used. In this case, six elements are used and thus the first three modes should be fairly accurate. Using elementary modal analysis, the first three modes of vibration are known to be 0.288 Hz , 0.877 Hz, and 9.82

Hz, respectively. This indicates percentage errors for the first three modes as 2.7%, 0.72%, and 13.1 % each. The diminishing accuracy with the increase in mode number is readily apparent due to a small number of elements in the model.

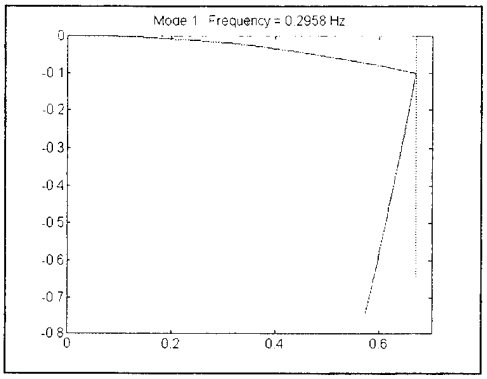

Figure 6.5. Modeshape for First Mode

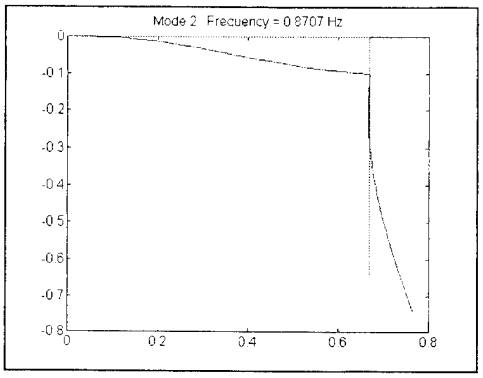

Figure 6.6. Modeshape for Second Mode

At this time it should be noted that the first finite element model consisted of twelve elements giving twenty-four natural modes. This first model's accuracy extended to the sixth natural mode before significant divergence was noticed. The problem encountered with the higher fidelity model was the introduction of uncontrollable and unobservable states. As discussed in Chapter III, the solution was to simplify the model to the current twelve mode model for the remainder of the thesis work.

Since the piezoceramic actuators use electro-mechanical coupling from an applied voltage to a strain on the beam, only a moment, or torque, may be applied as the control input. Based on the given modeshapes (eigenvectors) and the knowledge that the region of greatest torque is at the base for a fixed-free (cantilevered) configuration, it can be inferred that the optimal actuator and sensor placement be at the base of the structure and

at the base of the second arm. This configuration will give the greatest control input possible and also provide a nearly collocated sensor/actuator pair.

C. TRANSFORMATION TO MODAL FORM

Equation (6.10) is a damped free equation of motion derived from finite element analysis incorporating piezoceramic electro-mechanical coupling. Actually the FSS flexible arm has natural structural damping and in order to increase the fidelity of the model of our structure, the natural damping must be included. In order to add in the structural damping a linear transformation of the state must be used to get the model into *modal* form. *Modal* form is one that de-couples the equations into linearly independent first-order differential equations. In Chapter III, Section C., a method for a linear transformation of state is given. Using the generalized eigenvalue approach, there is a transformation matrix, Φ, that transforms equation (6.10) into diagonal form. The response of the system, in the absence of an external input is given by

$$\mathbf{M}\ddot{\mathbf{q}} + \mathbf{K}\mathbf{q} = \mathbf{0} \tag{6.12}$$

The transformation from physical or generalized coordinates, $\mathbf{q}$, to modal coordinates, ξ, is determined by the linear similarity transformation

$$\mathbf{q} = \Phi\xi \qquad \mathbf{T} = \Phi^{-1} \qquad \xi = \mathbf{T}\mathbf{q} \tag{6.13}$$

The desired equations of motion are of the form

$$\mathbf{M}\ddot{\mathbf{q}} + \mathbf{C}\dot{\mathbf{q}} + \mathbf{K}\mathbf{q} = \mathbf{0} \tag{6.14}$$

where **C** is the damping matrix for the system in physical coordinates. Combining equation (6.13) with equation (6.14) we obtain

$$\begin{gathered}\mathbf{M}\Phi\ddot{\xi} + \mathbf{C}\Phi\dot{\xi} + \mathbf{K}\Phi\xi = \mathbf{0} \\ \Phi^T\mathbf{M}\Phi\ddot{\xi} + \Phi^T\mathbf{C}\Phi\dot{\xi} + \Phi^T\mathbf{K}\Phi\xi = \mathbf{0}\end{gathered} \tag{6.15}$$

where F is determined so that

$$\Phi^T\mathbf{M}\Phi = \mathbf{I} \qquad \Phi^T\mathbf{C}\Phi = \begin{bmatrix} \ddots & & \\ & 2\zeta\omega_i & \\ & & \ddots \end{bmatrix} = [\Omega] \qquad \Phi^T\mathbf{K}\Phi = \begin{bmatrix} \ddots & & \\ & \omega_i^2 & \\ & & \ddots \end{bmatrix} = [\Lambda]$$

In this way, the equations of motion in modal coordinates become a set of de - coupled second - order differential equations

$$\ddot{\xi} + [\Omega]\dot{\xi} + [\Lambda]\xi = \mathbf{0} \tag{6.16}$$

which can be written in state - space form as

$$\ddot{\xi} = -[\Omega]\dot{\xi} - [\Lambda]\xi$$

$$\begin{Bmatrix} \dot{\xi} \\ \ddot{\xi} \end{Bmatrix} = \begin{bmatrix} \mathbf{0} & \mathbf{I} \\ -[\Lambda] & -[\Omega] \end{bmatrix} \begin{Bmatrix} \xi \\ \dot{\xi} \end{Bmatrix} = \mathbf{A}_m \{\xi\} \tag{6.17}$$

Using data obtained from previous experimentation on the FSS flexible arm, it was determined that the first two natural modes need 0.4% as the damping ratio and 10%

for the higher modes. These values are inserted into equation (6.17) and the equation is then transformed back to physical coordinates. Recalling equation (6.13c) a state-space transformation matrix can be obtained

$$\begin{Bmatrix} \xi \\ \dot{\xi} \end{Bmatrix} = \begin{bmatrix} \mathbf{T} & \mathbf{0} \\ \mathbf{0} & \mathbf{T} \end{bmatrix} \begin{Bmatrix} \mathbf{q} \\ \dot{\mathbf{q}} \end{Bmatrix} = [\mathbf{T}]\bar{\mathbf{q}} \tag{6.18}$$

thus the system matrix transformed back to physical coordinates is

$$[\mathbf{T}]\dot{\bar{\mathbf{q}}} = \mathbf{A}_m \mathbf{T}\bar{\mathbf{q}}$$

$$\dot{\bar{\mathbf{q}}} = [\mathbf{T}]^{-1}\mathbf{A}_m[\mathbf{T}]\bar{\mathbf{q}} \quad \Rightarrow \quad \dot{\bar{\mathbf{q}}} = \mathbf{A}\bar{\mathbf{q}} \tag{6.19}$$

where $\mathbf{A} = [\mathbf{T}]^{-1}\mathbf{A}_m[\mathbf{T}]$

D. STATE-SPACE REPRESENTATION

The analytical model of our system can be represented by the following state-space first-order coupled equations

$$\begin{aligned} \dot{\mathbf{x}} &= \mathbf{A}\mathbf{x} + \mathbf{B}\mathbf{u} + \mathbf{F}w \\ \mathbf{y} &= \mathbf{C}\mathbf{x} + v \end{aligned} \tag{6.20}$$

The system matrix, A, from equation (6.19) is now an accurate twenty-four state model approximating the actual FSS flexible arm assembly. The control matrix, B, based on equations (5.29) and (6.10), has two independent actuators and is a 24×2 matrix. The

sensor matrix, C, is a 6×24 matrix that contains two piezoceramic sensor outputs and four outputs from an optical infrared *VisionServer* camera system developed by *Real time Innovations, Inc.* [Ref. 6] The piezoceramic outputs are governed by equations (5.29) and (6.11). The *VisionServer* measures the displacements and rotations of the elbow and tip assemblies individually and outputs those four states directly. The plant uncertainty matrix, F, is initially the identity matrix and the model uncertainty is approximated at 5%. The sensor noise is taken as the squares of component rms noise values from documentation and previous research

VII. ANALYTICAL MODEL SIMULATION

In this chapter a LQG controller is designed using the methods discussed in Chapter III. The LQG controller will be designed to meet given performance criteria outlined in Section B of this chapter. The analytical model will be simulated using MATLAB and SIMULINK after which it will be ported to a VAXstation running MATRIXx to be tested on the real-time controller.

A. MODEL REPRESENTATION

From equation (6.20) the model is represented in state-space form as

$$\dot{\mathbf{x}} = \mathbf{A}\mathbf{x} + \mathbf{B}\mathbf{u} + \mathbf{F}w$$

$$\mathbf{y} = \mathbf{C}\mathbf{x} + v$$

The model is formed by the following components: the flexible body dynamics, the piezoceramic actuators, the piezoceramic sensors, and the *VisionServer* camera system[Ref. 6]. The type of controller to be designed is a regulator, i.e., there is no reference or commanded input to track, since the objective is to dampen all the oscillations in the system. The major disturbances are in the form of continuous and impact vibrations to the flexible arm, while secondary disturbances are the noise inputs to the sensors and actuators from the control system hardware. The state variables considered in the nominal model are the nodal displacements and nodal rotations, w and θ. The model upon which the LQG is designed combines the nominal plant, the estimated plant uncertainties, and the estimated process-noise model.

B. LQG DESIGN REQUIREMENTS

The primary objective is to damp out the effect of the disturbances as quickly as possible and maintain stability robustness. Specifically, the most important variable to minimize is the rotational displacement of the tip of the arm since this directly affects the performance of the antenna structure in space.

The FSS is setup for an initial condition response to simulate an impact disturbance input. The piezoceramic actuators are low authority controllers, and the time constant for settling out the disturbance will be on the order of five seconds. The steady state error to a continuous sinusoidal input is to be less than 0.1° for the tip assembly. In summary the performance objectives for the LQG controller are

Settling Time	**T_s < 20 seconds**	**(Time constant = 5 seconds)**
Steady State Error	**e_s < 0.1°**	**(Due to a sinusoidal input)**

C. PROPOSED DESIGN

The design of the LQG controller for this model is given by a combination of the solutions of the Linear Quadratic Regulator (LQR) and the Kalman Estimator (LQE) problem. The optimal control solution of the LQR problem which minimizes the performance index given by equation (3.6) is given by the state feedback equation

$$\mathbf{u} = -\mathbf{K}_{LQR}\mathbf{x} \tag{7.1}$$

where $\mathbf{K}_{LQR}$ is given by equation (3.7) provided that the state weighting matrix, **Q**, is symmetric and positive semi-definite, the control weighting matrix, **R**, is symmetric and positive definite, and the pair (**A**,**B**) is controllable, with the controllability matrix given by equation (3.14a). Since the sensors do not measure all the states, it is desirable to transform equation (3.6) into an output dependent equation so as to have direct influence over the weighting parameters. The cost function, in general given as

$$J = \int (\mathbf{x}^T \mathbf{Q}\mathbf{x} + \mathbf{u}^T \mathbf{R}\mathbf{u}) dt$$

can be adapted to the case when we penalize the output, **y**. Using the fact that $\mathbf{y}=\mathbf{C}\mathbf{x}$ and $\mathbf{y}^T=\mathbf{x}^T\mathbf{C}^T$, another matrix, $\mathbf{Q}_y$ can be defined where $\mathbf{C}^T\mathbf{Q}_y\mathbf{C}$, and substitution into the above equation yields

$$J = \int (\mathbf{y}^T \mathbf{Q}_y \mathbf{y} + \mathbf{u}^T \mathbf{R}\mathbf{u}) dt \qquad (7.2)$$

which has an explicit dependence on the sensor outputs.

The solution to the LQR seeks a compromise between minimum energy (control input) and best performance. For an antenna structure in space it is desirable to minimize the beam losses incurred due to the disturbance inputs. Similarly, in this model the priority is to minimize the tip deflection and rotation so we will penalize those outputs more heavily than the others. In order to keep the output of the piezoceramic sensors within limitations a penalty must be imposed on those outputs as well.

Using SIMULINK, a dynamical model was created and simulated. Figure (7.1) is the block diagram of the simulation model.

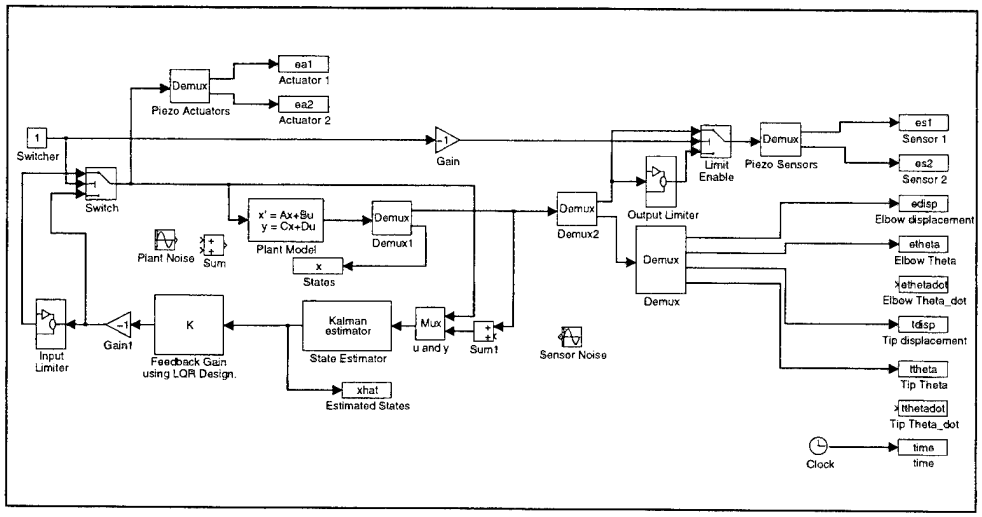

Figure 7.1. SIMULINK Block Diagram

D. SIMULATION AND RESULTS

From simulation, the values of $\mathbf{Q}_y$, the output weighting matrix, and $\mathbf{R}$, the control weighting matrix, were iteratively determined to be

$$\mathbf{Q}_y = \begin{bmatrix} 100 & 0 & 0 & 0 & 0 & 0 \\ 0 & 100 & 0 & 0 & 0 & 0 \\ 0 & 0 & 1 & 0 & 0 & 0 \\ 0 & 0 & 0 & 1 & 0 & 0 \\ 0 & 0 & 0 & 0 & 9000 & 0 \\ 0 & 0 & 0 & 0 & 0 & 900000 \end{bmatrix} \qquad \mathbf{R} = \begin{bmatrix} 0.1 & 0 \\ 0 & 0.1 \end{bmatrix} \tag{7.3}$$

where the sensor output vector, $\mathbf{y}$, contains the piezoceramic sensors as the first two elements and four VisionServer outputs (elbow displacement, elbow rotation, tip

displacement, and tip rotation) as the last four elements of the output vector. The two control inputs are the base actuator and the elbow actuator, respectively.

These values kept the control inputs within their limitations of ±150 volts, the sensors within their limitations of ±10 volts, minimized the steady state error, and met the settling time constraints. Figure 7.2 illustrates a typical tip rotational displacement in the time domain, it is representative of all sensor data observed. Appendix C contains the simulation results for all the sensors.

Another method for determining the performance of the LQG controller is to measure the damping effectiveness for the system. A good method for determining the damping from simulations is the Log Decrement method given by

$$\varsigma = \frac{1}{2\pi n} \ln\left(\frac{A_i}{A_f}\right) \tag{7.4}$$

with ζ being the damping ratio, n the number of cycles between measurements, A_i and A_f the initial and final amplitudes, respectively. In order to determine damping, we need to excite one mode at a time. In general, we were able to excite independently only the first two modes.

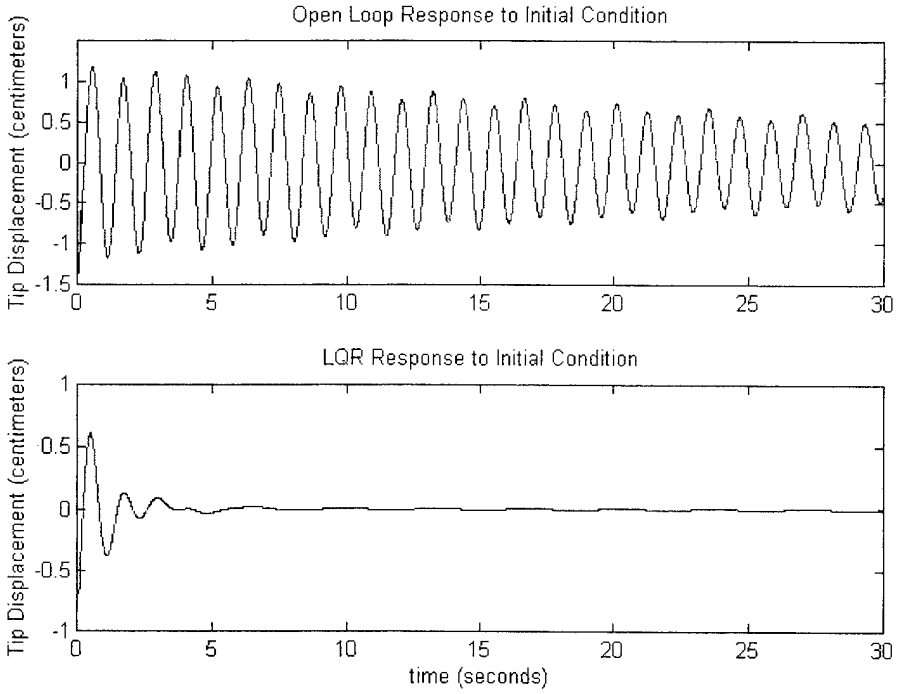

Figure 7.2. Tip Rotational Displacement Initial Condition Response

The damping coefficient for the first two modes determined from the simulation results by the log decrement method is 12%. Recalling the original damping ratio of 0.4% an increase in damping on the order of 29 times or 2,900% is obtained.

The next step is to design the Kalman filter. The solution to the optimal state estimator is given by equation (3.9) where the observer gain is taken from equation (3.11). Equation (3.11) has a solution provided that **W**, the plant uncertainty variance matrix, is symmetric and positive semidefinite; the sensor noise variance matrix, **V**, is symmetric and positive definite, and the pair (**A**,**C**) is observable where the observability matrix is given by equation (3.14b). The values determined from hardware documentation for the sensors, and previous research for the plant uncertainty model and process-noise model are given below. Of note is the fact that the piezoceramic sensors

generate a clean signal that has very little noise and that is reflected in the corresponding variance matrix.

$$\mathbf{W} = 0.01[\mathbf{I}] \qquad \mathbf{V} = \begin{bmatrix} 0.0001 & 0 & 0 & 0 & 0 & 0 \\ 0 & 0.0001 & 0 & 0 & 0 & 0 \\ 0 & 0 & 0.00025 & 0 & 0 & 0 \\ 0 & 0 & 0 & 0.002 & 0 & 0 \\ 0 & 0 & 0 & 0 & 0.00025 & 0 \\ 0 & 0 & 0 & 0 & 0 & 0.001 \end{bmatrix} \tag{7.4}$$

The designs for the LQR controller and the Kalman filter were been performed individually. To create the compensator for the system, we must combine the two together into one system. Using equation (3.9), the estimator equation, we will introduce the controller equation (7.1) for the control input modified for the estimated states rather than the actual states

$$\dot{\hat{\mathbf{x}}} = \mathbf{A}\mathbf{x} + \mathbf{B}\mathbf{u} + \hat{\mathbf{L}}(\mathbf{y} - \mathbf{C}\hat{\mathbf{x}})$$

$$\mathbf{u} = -\mathbf{K}_{\mathbf{LQR}}\hat{\mathbf{x}}$$

Substituting the control equation into the estimator equation we arrive at the overall compensator equation

$$\begin{aligned} \dot{\hat{\mathbf{x}}} &= (\mathbf{A} - \mathbf{B}\mathbf{K}_{\mathbf{LQR}} - \hat{\mathbf{L}}\mathbf{C})\hat{\mathbf{x}} + \hat{\mathbf{L}}\mathbf{y} \\ \mathbf{u} &= -\mathbf{K}_{\mathbf{LQR}}\hat{\mathbf{x}} \end{aligned} \tag{7.5}$$

with the inputs to the compensator being the sensor outputs, **y**, and the outputs of the compensator as the control input to the structural system ,**u**.

The response using this LQG controller can be expected to converge to the LQR response over time. The speed of convergence is a reflection of the estimator's time constant. Figure 7.3 illustrates the error between the LQR response and the LQG response due to the Kalman filter. From Figure 7.3 it can be seen that the LQG response is less effective than the LQR due to the loss of robustness with the introduction of the uncertainty and noise into the system.

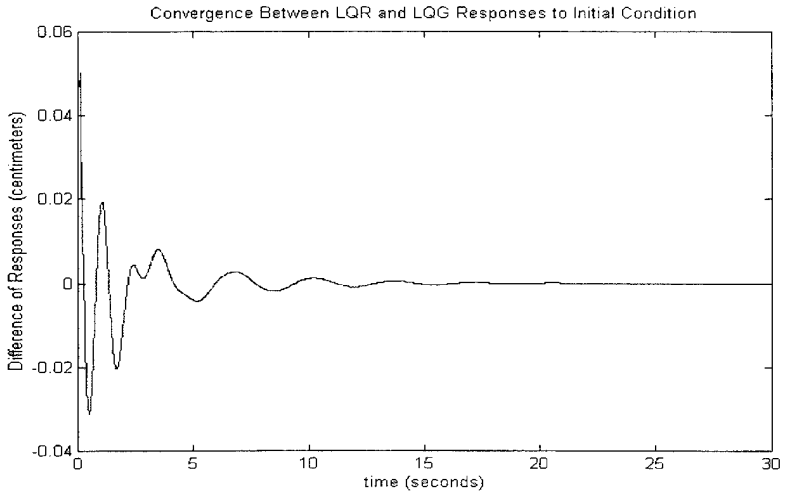

Figure 7.3. Convergence of LQG to the LQR Initial Condition Response.

The value for the initial condition, the tip displaced by 3 centimeters, was determined experimentally by defining the maximum deflection that would keep the voltage input to the controller by the piezoceramic sensors within limits (±10 volts).

The final step in the design process for the LQG controller is to discretize the system for the experimental verification effort. The method of discretization to be used is

the Tustin transformation. The relationship between the continuous domain (s-domain) and the discrete domain (z-domain) is given by

$$z = e^{sT} \tag{7.6}$$

where T is the sampling period. A Tustin transformation maintains the frequency response of the continuous system while preserving the mapping of the s-plane into the z-plane The Tustin transformation is a Pade approximation to the exponential, equation (7.6). [Ref. 7, pp. 253-282]

$$z = \frac{1 + \frac{sT}{2}}{1 - \frac{sT}{2}} \tag{7.7}$$

The continuous system will be transformed to the discrete domain using a sampling period of 0.01 seconds (100 Hz). The tip response for the LQG controller in the discrete domain is shown in Figure 7.4, note the similarity between the continuous response and the discrete response.

The implementation on the real hardware is shown in [Ref. 8]. The controller is implemented in software on the VAXstation 3100 using MATRIXx and SystemBuild. The real-time code is then downloaded to the AC-100 real-time controller for experimental verification of this design.

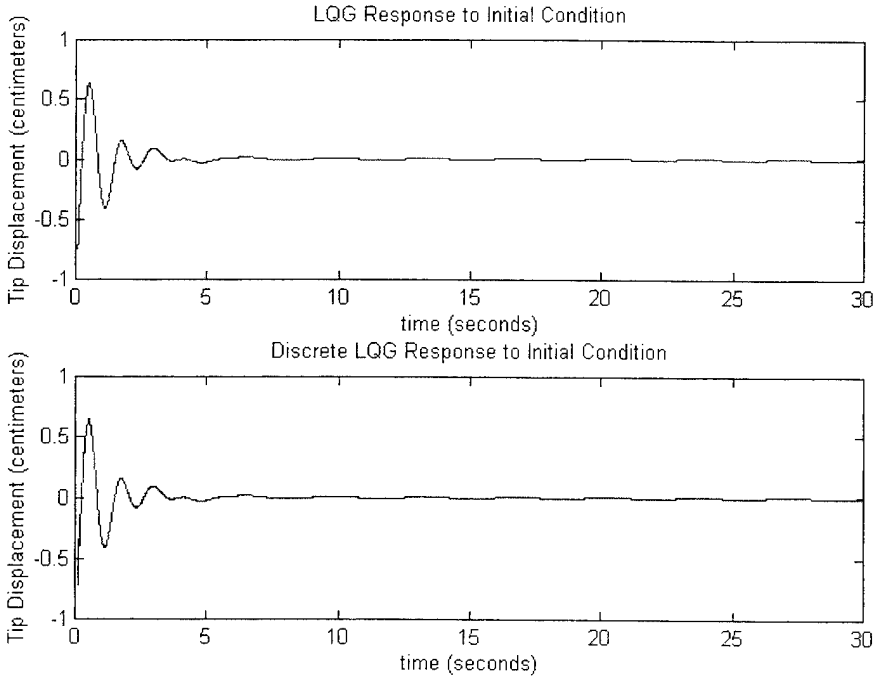

Figure 7.4. Comparison Between the LQG Continuous and Discrete Responses

VIII. CONCLUSIONS AND RECOMMENDATIONS

A. SUMMARY

This thesis presents the design of an optimal controller for a flexible spacecraft structure model using Linear Quadratic Gaussian techniques with piezoceramic actuators and sensors. An optical sensor package is also introduced into the system to provide control inputs.

A finite element model of the structure was provided that accounted for the electro-mechanical coupling effects of the piezoceramic devices. The finite element model was enhanced by the addition of structural damping. The design of the Linear Quadratic Gaussian controller is based on the combination of the Linear Quadratic Regulator (LQR) solution and the optimal estimator problem (Kalman filter). The solution to the LQR problem was transformed from a state dependent problem to a output dependent problem. This technique allowed for the direct control over the control inputs in relation to the sensor outputs. The plant uncertainty and process-noise matrices were determined by iteration using the sensor specifications and previous research as the starting points and then fine-tuning each of the matrices' elements to achieve the desired performance. The estimator and LQR controller were combined to form the LQG controller and subjected to rigorous continuous-time simulation in Matlab and SIMULINK.

The model was then transformed to discrete space via a Tustin transformation following the continuous-time simulations. The discrete controller was also simulated in

Matlab to ensure a stable introduction into the experimental setup with the real-time controller, AC-100.

B. CONCLUSIONS

In this study a Linear Quadratic Gaussian controller was designed and developed for the Flexible Spacecraft Simulator (FSS) at the Naval Postgraduate School. All specifications for the FSS were met to include the sensor and actuator limitations for the real-time controller. The controller responded to a initial condition disturbance and met the time requirements and steady state error requirements specified in the design criteria. A significant increase in damping on the order of 2900% was achieved with the LQG controller. The optimal estimator's performance met specifications, but only marginally due to the fact that some of the states had small observability values. This condition may have severe control implications when implemented experimentally.

C. RECOMMENDATIONS

The LQG controller design should be verified experimentally by testing with the FSS flexible structure [Ref. 8]. The finite element method for characterizing the structure is good for approximation only, and the use of modal analysis would increase the fidelity of the model. Further study in the use of Loop Transfer Recovery techniques for this controller can recover some of the loss in robustness, but this is at the price of losing nominal performance.

IX. REFERENCES

1. Friedland, B., *Control System Design*, McGraw-Hill, New York, 1986.

2. Franklin, G., Powell, J., and Emami-Naeini, A., *Feedback Control of Dynamic Systems*, Chapter 7, Addison-Wesley, Menlo Park, CA, 1994.

3. Z. Chaudhry and C. Rogers, Actuators for Smart Structures, *Fiber Optic Smart Structures*, pp. 497-505, Wiley, New York, 1995.

4. B. Jaffe, R. S. Roth, and S. Marzullo, Piezoelectric Properties of Lead Zirconate-Lead Titanate Solid Solution Ceramics, *Journal of Applied Physics* **25**, 809-810 (1954).

5. Meirovitch, L., *Elements of Vibration Analysis*, pp. 300-312, McGraw-Hill, New York, 1986.

6. Real Time Innovations, Inc., VisionServer Real-Time Vision System, User's Guide, 1992.

7. Shahian,B. and Hassul, M., *Control System Design Using Matlab*, Prentice-Hall, Englewood Cliffs, NJ, 1993.

8. Harrington, W., "Experimental Verification of an Optimal Linear Controller on a Flexible Structure", Engineer's Thesis, Naval Postgraduate School, December 1995.

APPENDIX A

FINITE ELEMENT MODEL MATLAB CODE

```
%%Finite EleMent Model PrograM for the FSS
%%
%%This prograM characterizes the FSS flexible appendage.
%%LCDR Bill Harrington, USN  October 1995
%%
%%The flexible appendage is to be Modeled as a 6 eleMent FEM with
%%piezoceraMic actuators located on eleMents 1 and 4, and piezoceraMic
%%sensors located on eleMents 2 and 5.  The elbow and tip will be treated as
%%rigid body Masses.
%%
%%
%%This Model assuMes 0.5% structural daMping, and will solve for the first
%%12 natural Modes.  The degree of accuracy is suitable only for the
%%first 3 Modes (half the nuMber of eleMents, normally).
%%

clear
clc
format short e
global A B C D

%%structural properties

nuMeleMents=6;
h=[0.07 0.03 0.5688 0.07 0.03 0.549];                    %%Meters
thicKness=0.0015875;
height=0.0254;
rho=2800;                                                %%Kg/M^3
elMass=rho*height*thicKness;                             %%Mass/length
elinertia=1/12*thicKness^3*height;                  %%Meter^4
E=72e9;                                                  %%Modulus of elasticity

%%CoMpute eleMental stiffness and Mass Matrices

KeleMent=0*ones(4,4*nuMeleMents);
MeleMent=0*ones(4,4*nuMeleMents);

for i=1:nuMeleMents,...
        KeleMent(:,4*i-3:4*i)=E*elinertia/h(i)^3*[12 6*h(i) -12 6*h(i);...
        6*h(i) 4*h(i)^2 -6*h(i) 2*h(i)^2;-12 -6*h(i) 12 -6*h(i);...
        6*h(i) 2*h(i)^2 -6*h(i) 4*h(i)^2];
end

for i=1:nuMeleMents,...
        MeleMent(:,4*i-3:4*i)=elMass*h(i)/420*[156 22*h(i) 54 -13*h(i);...
        22*h(i) 4*h(i)^2 13*h(i) -3*h(i)^2;54 13*h(i) 156 -22*h(i);...
        -13*h(i) -3*h(i)^2 -22*h(i) 4*h(i)^2];
end
```

```
%%Construct global Mass and stiffness Matrices

M=0*ones(2*(nuMeleMents+1));
K=0*ones(2*(nuMeleMents+1));

for i=1:nuMeleMents,...
        M(2*i-1:2*i+2,2*i-1:2*i+2)=M(2*i-1:2*i+2,2*i-1:2*i+2) +MeleMent(:,4*i-3:4*i);
end

for i=1:nuMeleMents,...
        K(2*i-1:2*i+2,2*i-1:2*i+2)=K(2*i-1:2*i+2,2*i-1:2*i+2) +KeleMent(:,4*i-3:4*i);
end

%%Clean up
clear elinertia;

%%Fix for fixed boundry condition (row,coluMns 1&2 =0)

M=M(3:2*(nuMeleMents+1),3:2*(nuMeleMents+1));
K=K(3:2*(nuMeleMents+1),3:2*(nuMeleMents+1));

M(5,5:8)=M(5,5:8)-MeleMent(1,13:16);
M(6:8,5)=M(6:8,5)-MeleMent(2:4,13);

K(5,5:8)=K(5,5:8)-KeleMent(1,13:16);
K(6:8,5)=K(6:8,5)-KeleMent(2:4,13);


clear KeleMent MeleMent;

%%Now add elbow and tip Masses.

Melbow=0.40823;
Mtip=0.37648;
MbeaM2=(h(1)+h(2)+h(3))*elMass;

M(5,5)=M(5,5)+Melbow+MbeaM2+Mtip;
M(11,11)=M(11,11)+Mtip;

clear Mpoint Melbow Mtip ipoint MbeaM2;

%%Define the piezo actuator and sensor eleMents

delta=thicKness/2;
tp=2*1.905e-4;
wp=0.02;
Ep=6.3e10;
d31=-1.8e-10;
eT3=1.5e-8;
rhop=7700;
Kpiezo=wp*tp*Ep*(delta^2 + delta*tp + (tp^2)/3);

Ka=Kpiezo/h(1)*[12/h(1)^2 6/h(1) -12/h(1)^2 6/h(1);...
6/h(1) 4 -6/h(1) 2;-12/h(1)^2 -6/h(1) 12/h(1)^2 -6/h(1);...
6/h(1) 2 -6/h(1) 4];
```

```
Ks=Kpiezo/h(2)*[12/h(2)^2 6/h(2) -12/h(2)^2 6/h(2);...
6/h(2) 4 -6/h(2) 2;-12/h(2)^2 -6/h(2) 12/h(2)^2 -6/h(2);...
6/h(2) 2 -6/h(2) 4];

Mp=rhop*wp*tp;                                          %%Mass/length piezo

Ma=Mp*h(1)/420*[156 22*h(1) 54 -13*h(1);22*h(1) 4*h(1)^2 13*h(1) -3*h(1)^2;...
54 13*h(1) 156 -22*h(1);-13*h(1) -3*h(1)^2 -22*h(1) 4*h(1)^2];

Ms=Mp*h(2)/420*[156 22*h(2) 54 -13*h(2);22*h(2) 4*h(2)^2 13*h(2) -3*h(2)^2;...
54 13*h(2) 156 -22*h(2);-13*h(2) -3*h(2)^2 -22*h(2) 4*h(2)^2];

%%Add the piezo eleMent Mass and stiffness Matrices to the structure

M(1:2,1:2)=M(1:2,1:2)+2*Ma(3:4,3:4);
M(1:4,1:4)=M(1:4,1:4)+2*Ms;
M(6:8,6:8)=M(6:8,6:8)+2*Ma(2:4,2:4);
M(7:10,7:10)=M(7:10,7:10)+2*Ms;

K(1:2,1:2)=K(1:2,1:2)+2*Ka(3:4,3:4);
K(1:4,1:4)=K(1:4,1:4)+2*Ks;
K(6:8,6:8)=K(6:8,6:8)+2*Ka(2:4,2:4);
K(7:10,7:10)=K(7:10,7:10)+2*Ks;

clear Ks Ka Ms Ma Kpiezo;

%%Solve for natural frequencies and Mode shapes.

[oMega2,Phi,Psi]=eign(K,M);
oMega=sqrt(oMega2);
Hertz=oMega/2/pi;
ttl=str2mat('   Omega','Hertz','       ');
[ttl(1,:) ttl(3,:) ttl(2,:)]
[oMega Hertz]

%%Construct the a,b,c, and d Matrices for state-space forM.

%%Need More info on the piezos.

bb1=0; bb2=-d31*Ep*wp*(delta +tp/2); bb3=0; bb4=-bb2;
gaMMa=wp*h(2)/tp*(eT3-d31^2*Ep);
b1=[bb3 bb4 0 0 0 0 0 0 0 0 0 0];
b2=[0 0 0 0 bb1 bb2 bb3 bb4 0 0 0 0];
btMp=[b1' b2']; btMp2=-2*inv(M)*btMp;  btMp3=-2*Phi'*btMp;
ctMp=[bb1 bb2 bb3 bb4 zeros(1,20)]/gaMMa;                    %sensor 1
ctMp2=[0 0 0 0 0 0 bb1 bb2 bb3 bb4 0 0 zeros(1,12)]/gaMMa;   %sensor 2
ctMp3=[0 0 0 0 1 0 zeros(1,18)];                             %e. disp.
ctMp4=[0 0 0 0 0 -1 zeros(1,18)];                            %e. rot.
ctMp5=[zeros(1,10) 1 0 zeros(1,12)];                         %t. disp.
ctMp6=[zeros(1,10) 0 -1 zeros(1,12)];                        %t. rot.

a=[0*ones(12) eye(12);-inv(M)*K 0*ones(12)];
b=[0*ones(12,2);btMp2];
c=[ctMp;ctMp2;ctMp3;ctMp4;ctMp5;ctMp6];                      %observation matrix
d=0*ones(6,2);
```

```
clear bb1 bb2 bb3 bb4 gaMMa b1 b2 btMp ctMp;
clear ctMp2 ctMp3 ctMp4 ctMp5 ctMp6 ctMp7 ctMp8;
clear E Ep eT3 i;
clear btMp2 cx d31 delta e elMass ep et3 height Mp rho rhop;
clear thicKness tp wp

%%Construct transformation matrix from modal to physical coordinates.

Phi_inv=inv(Phi);
PPhi=zeros(24);
PPhi(1:12,1:12)=Phi_inv;
PPhi(13:24,13:24)=Phi_inv;

PPhi_inv=inv(PPhi);

%%Insert natural structural damping, 0.5% for first two modes then 20% for rest.

damp=-2*0.005*oMega(1:2);damp2=-2*0.1*oMega(3:12); damp3=diag([damp' damp2']);
a2=[zeros(12) eye(12);-diag(oMega2) damp3];
b2=[zeros(12,2);btMp3];
c2=[c(:,1:12) zeros(6,12)]*[Phi zeros(size(Phi));zeros(size(Phi)) Phi];
d2=d;

a2m=PPhi_inv*a2*PPhi;
A=clean(a2m,1e-6);
b2m=PPhi_inv*b2;
B=clean(b2m,1e-6);
c2m=c2*PPhi;
C=clean(c2m,1e-7);
D=d;

%%Set an initial condition (tip displaced by 3 cm)
x0=[0 0 0 0 0.02 0 0 0 0 0 -0.03 0 zeros(1,12)];

%%Time vector, t
t=0:0.01:30;

disp('Initialization of variables complete for two beam analysis. (FEM3)')
```

APPENDIX B

ANALYTICAL MODEL MODESHAPES

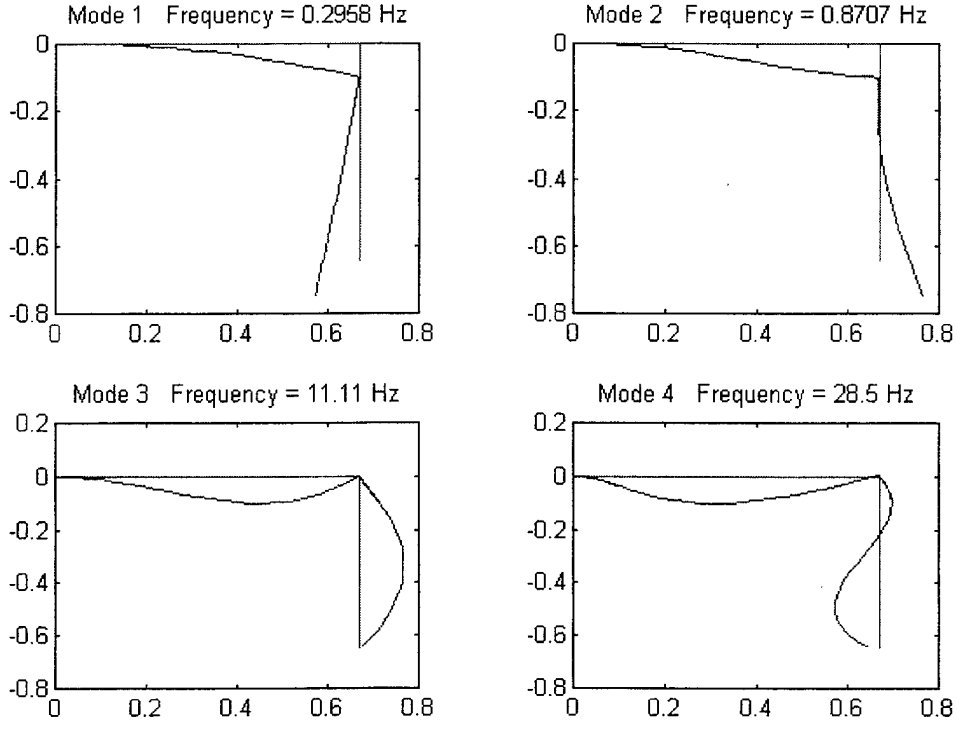

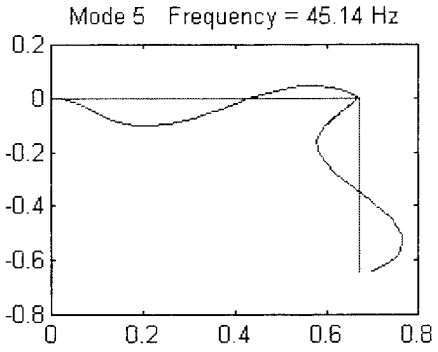
Mode 5 Frequency = 45.14 Hz
0.2
0
-0.2
-0.4
-0.6
-0.8
0
0.2
0.4
0.6
0.8

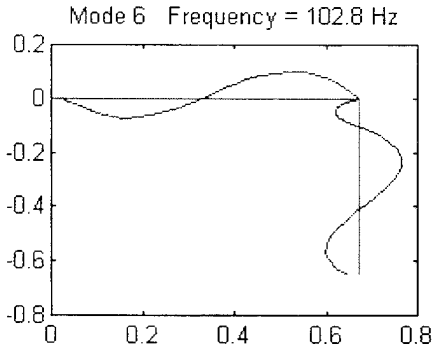
Mode 6 Frequency = 102.8 Hz
0.2
0
-0.2
-0.4
-0.6
-0.8
0
0.2
0.4
0.6
0.8

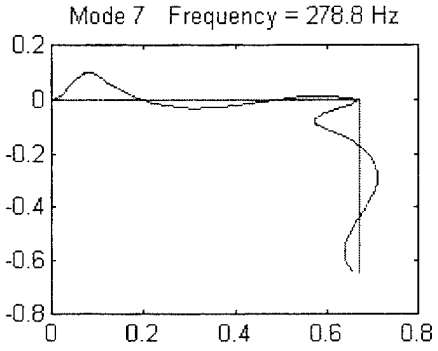
Mode 7 Frequency = 278.8 Hz
0.2
0
-0.2
-0.4
-0.6
-0.8
0
0.2
0.4
0.6
0.8

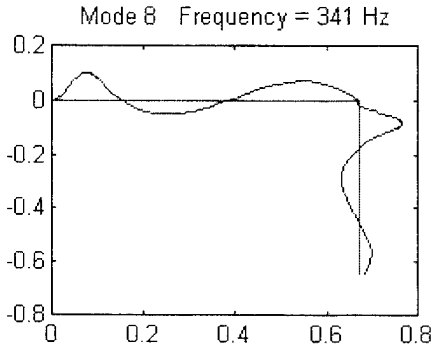
Mode 8 Frequency = 341 Hz
0.2
0
-0.2
-0.4
-0.6
-0.8
0
0.2
0.4
0.6
0.8

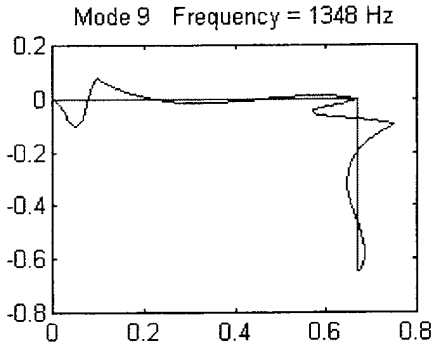
Mode 9 Frequency = 1348 Hz
0.2
0
-0.2
-0.4
-0.6
-0.8
0
0.2
0.4
0.6
0.8

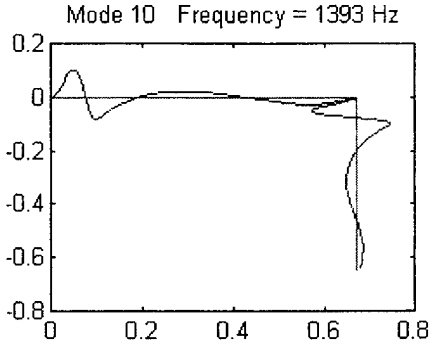
Mode 10 Frequency = 1393 Hz
0.2
0
-0.2
-0.4
-0.6
-0.8
0
0.2
0.4
0.6
0.8

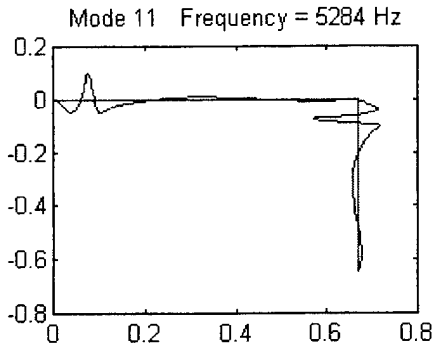
Mode 11 Frequency = 5284 Hz
0.2
0
-0.2
-0.4
-0.6
-0.8
0
0.2
0.4
0.6
0.8

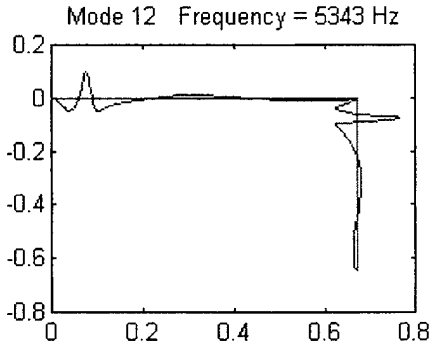
Mode 12 Frequency = 5343 Hz
0.2
0
-0.2
-0.4
-0.6
-0.8
0
0.2
0.4
0.6
0.8

APPENDIX C

SENSOR OUTPUTS FOR LQG CONTROLLER

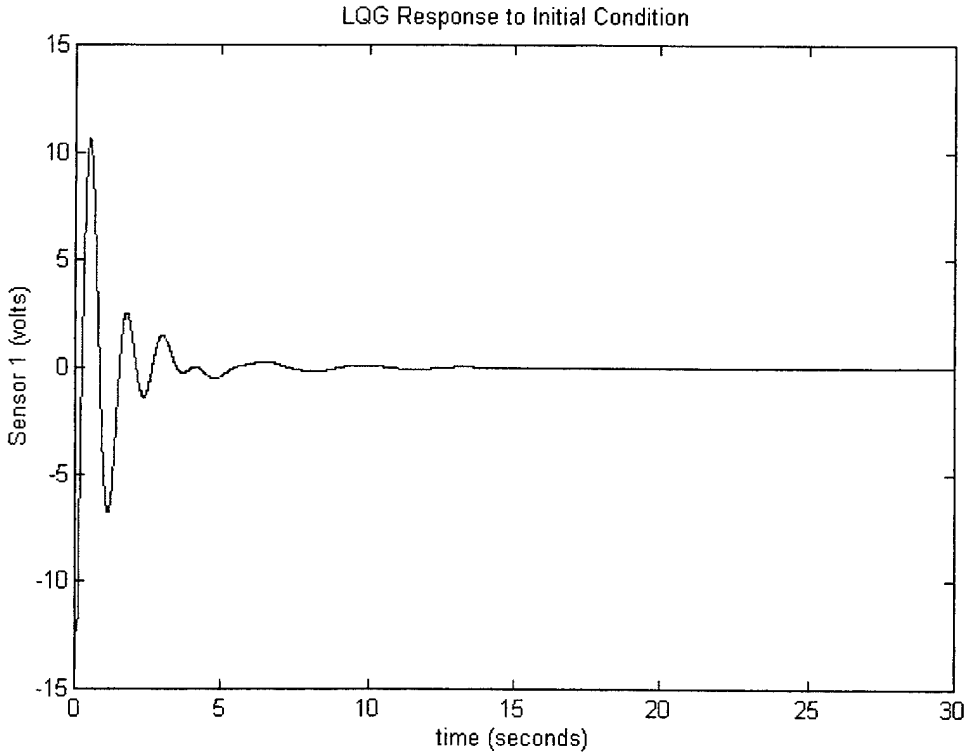

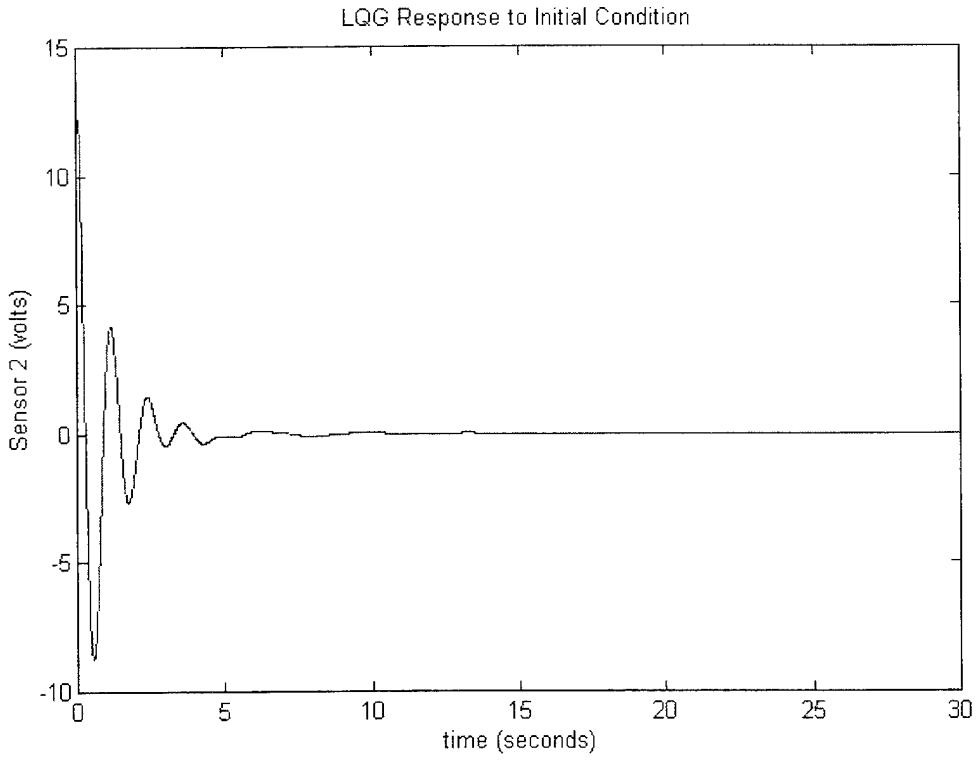
LQG Response to Initial Condition
Sensor 2 (volts)
time (seconds)
15
10
5
0
-5
-10
0
5
10
15
20
25
30

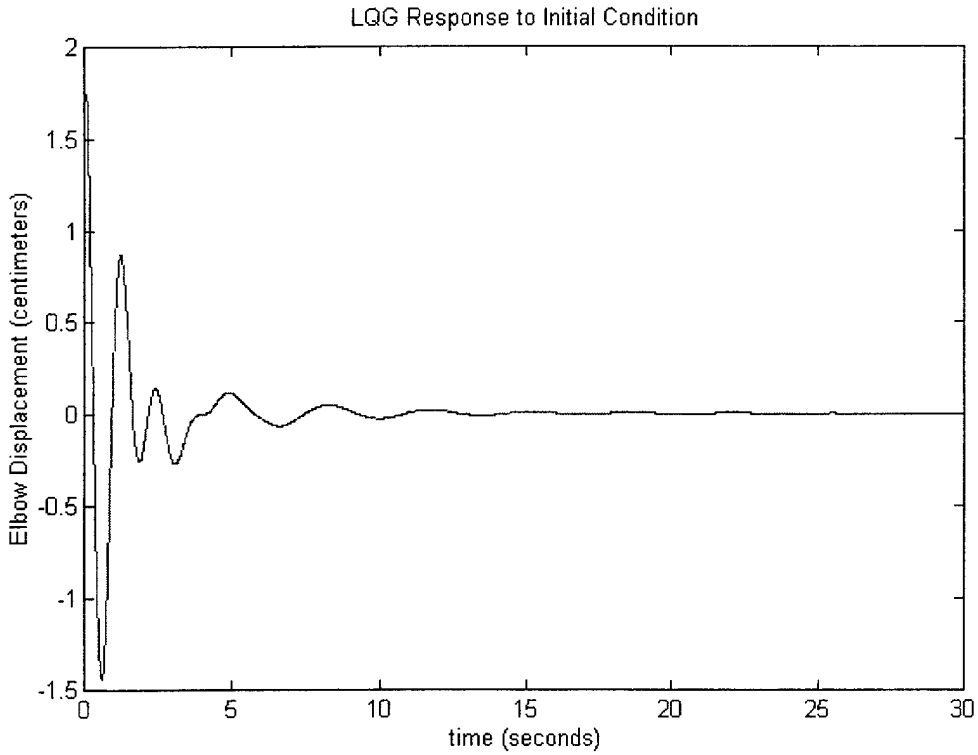
LQG Response to Initial Condition
Elbow Displacement (centimeters)
time (seconds)
2
1.5
1
0.5
0
-0.5
-1
-1.5
0
5
10
15
20
25
30

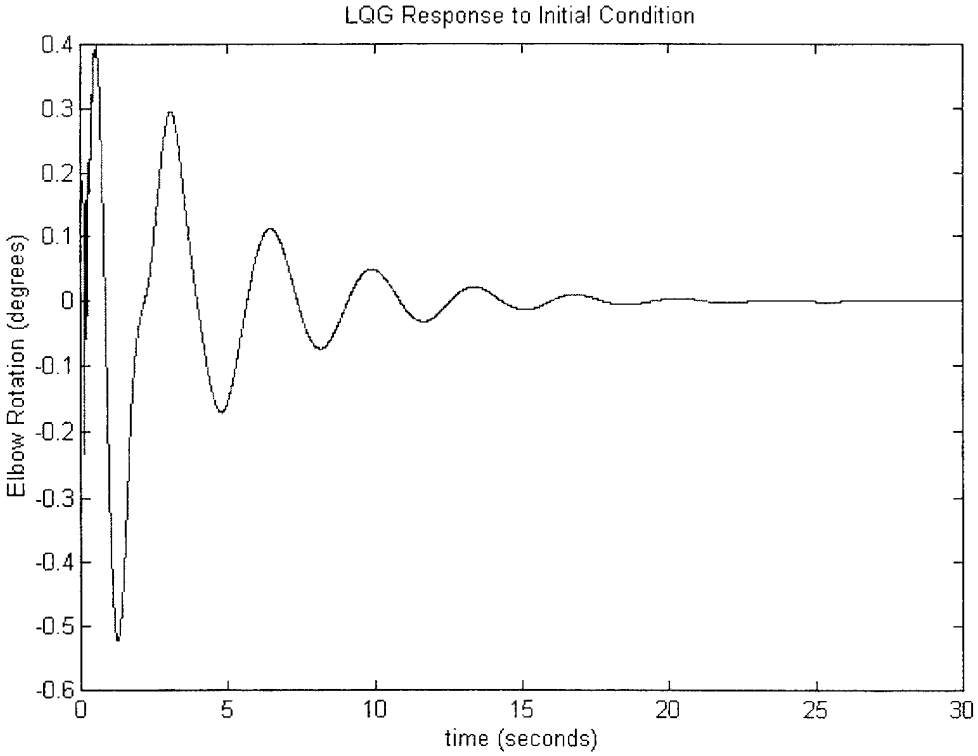
LQG Response to Initial Condition
Elbow Rotation (degrees)
time (seconds)
0.4
0.3
0.2
0.1
0
-0.1
-0.2
-0.3
-0.4
-0.5
-0.6
0
5
10
15
20
25
30

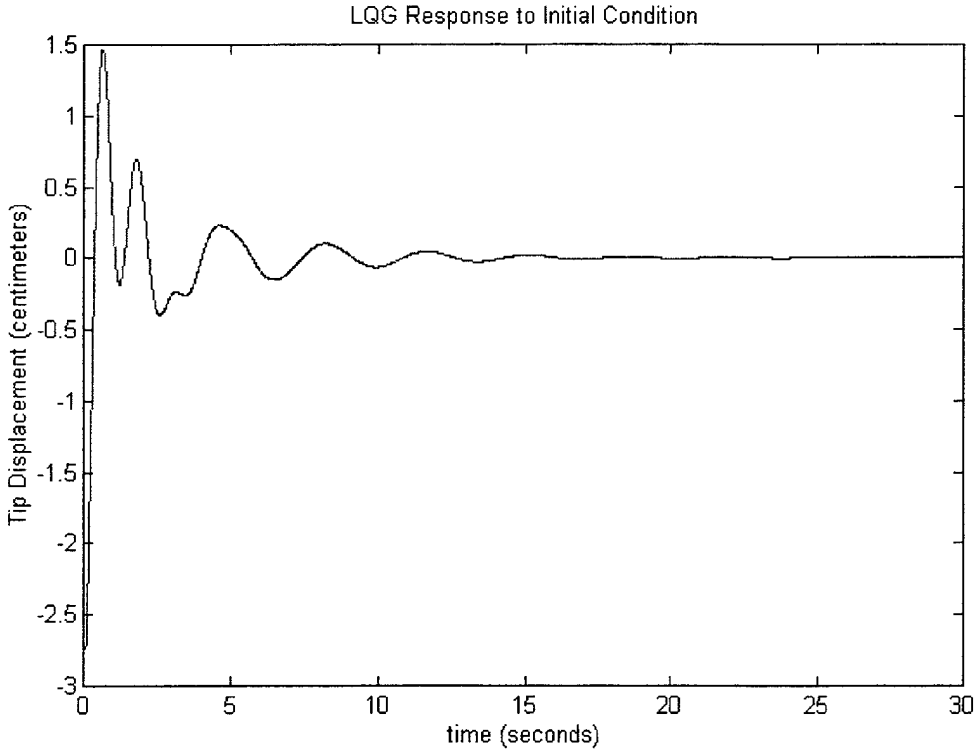
LQG Response to Initial Condition
Tip Displacement (centimeters)
time (seconds)
1.5
1
0.5
0
-0.5
-1
-1.5
-2
-2.5
-3
0
5
10
15
20
25
30

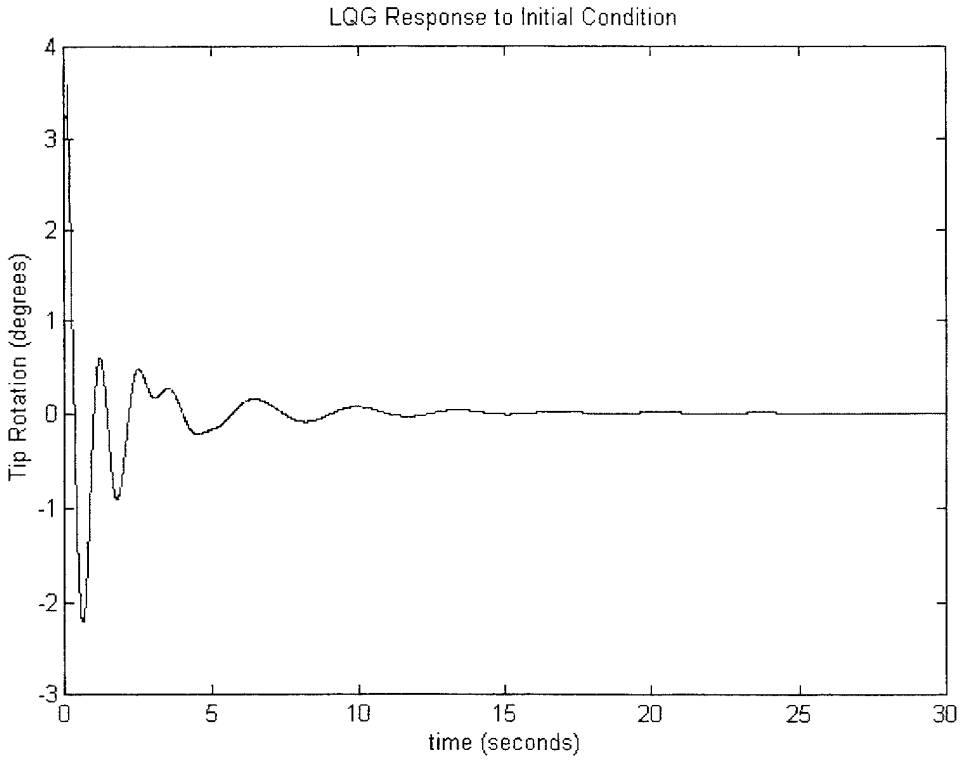
LQG Response to Initial Condition
Tip Rotation (degrees)
time (seconds)
4
3
2
1
0
-1
-2
-3
0
5
10
15
20
25
30

INITIAL DISTRIBUTION LIST

		No. Copies
1.	Defense Technical Information Center 8725 John J. Kingman Rd., STE 0944 Ft. Belvoir, VA 22060-6218	2
2.	Library, Code 013 Naval Postgraduate School Monterey, CA 93943-5101	2
3.	Chairman, Code EC Department of Electrical and Computer Engineering Naval Postgraduate School Monterey, CA 93943-5121	1
4.	Chairman, Code SP Space Systems Academic Group Naval Postgraduate School Monterey, CA 93943-5110	1
5.	Professor Roberto Cristi, Code EC/Cx Department of Electrical and Computer Engineering Naval Postgraduate School Monterey, CA 93943-5121	2
6.	Professor Brij N. Agrawal, Code AA/Ag Department of Aeronautical and Astronautical Engineering Naval Postgraduate School Monterey, CA 93943-5106	2
7.	Professor John L. Meyer, Code AA/My Department of Aeronautical and Astronautical Engineering Naval Postgraduate School Monterey, CA 93943-5106	1
8.	Commander, Naval Space Command Attn: N112 5280 4th Street Dahlgren, VA 22448-5300	1

9. Assistant Commander for Space Technology — 1
Naval Research Laboratory
Code 9110
Attn: Lieutenant Commander Barbara Bell
4555 Overlook Ave. SW
Washington, DC 20375-5000

10. Captain Thomson — 1
Office of the Chief of Naval Operations
Code N63, Room 4E679, The Pentagon
Washington, DC 20350-2000

11. Assistant Commander for Space Technology — 2
Naval Research Laboratory
Code 9110
Attn: Lieutenant Commander William B. Harrington, Jr.
4555 Overlook Ave. SW
Washington, DC 20375-5000